REPORT DOCUMENTATION PAGE

Form Approved
OMB No. 0704-0188

1. AGENCY USE ONLY (Leave blank)	2. REPORT DATE	3. REPORT TYPE AND DATES COVERED
		Final Report/Oct 88 - Oct 89

4. TITLE AND SUBTITLE

Soft X-ray Laser Development

5. FUNDING NUMBERS

61102F/2301/A8

6. AUTHOR(S)

Szymon Suckewer

7. PERFORMING ORGANIZATION NAME(S) AND ADDRESS(ES)

Princeton University
Plasma Physics Laboratory
Princeton, NY 08544

8. PERFORMING ORGANIZATION REPORT NUMBER

AFOSR-TR- 90 0881

9. SPONSORING/MONITORING AGENCY NAME(S) AND ADDRESS(ES)

AFOSR/NP
Bolling AFB DC 20332-6448

10. SPONSORING/MONITORING AGENCY REPORT NUMBER

AFOSR-86-0066

11. SUPPLEMENTARY NOTES

12a. DISTRIBUTION/AVAILABILITY STATEMENT

Approved for public release; distribution is unlimited.

12b. DISTRIBUTION CODE

13. ABSTRACT (Maximum 200 words)

A 3mJ, 182-Anstrom soft x-ray laser abased on a recombining plasma was created with an efficiency almost two orders of magnitude higher than the collisionally-pumped Livermore device. In addition, an amplifier section was added, consisting of a 3mm long carbon plasma which yielded a gain of 8 per cm.

14. SUBJECT TERMS

soft x-ray, plasma, pumped laser.

15. NUMBER OF PAGES

45

16. PRICE CODE

17. SECURITY CLASSIFICATION OF REPORT	18. SECURITY CLASSIFICATION OF THIS PAGE	19. SECURITY CLASSIFICATION OF ABSTRACT	20. LIMITATION OF ABSTRACT
UNCLASSIFIED	UNCLASSIFIED	UNCLASSIFIED	UL SAR

GENERAL INSTRUCTIONS FOR COMPLETING SF 298

The Report Documentation Page (RDP) is used in announcing and cataloging reports. It is important that this information be consistent with the rest of the report, particularly the cover and title page. Instructions for filling in each block of the form follow. It is important to ***stay within the lines*** to meet ***optical scanning requirements.***

Block 1. Agency Use Only *(Leave blank)*.

Block 2. Report Date. Full publication date including day, month, and year, if available (e.g. 1 Jan 88). Must cite at least the year.

Block 3. Type of Report and Dates Covered. State whether report is interim, final, etc. If applicable, enter inclusive report dates (e.g. 10 Jun 87 - 30 Jun 88).

Block 4. Title and Subtitle. A title is taken from the part of the report that provides the most meaningful and complete information. When a report is prepared in more than one volume, repeat the primary title, add volume number, and include subtitle for the specific volume. On classified documents enter the title classification in parentheses.

Block 5. Funding Numbers. To include contract and grant numbers; may include program element number(s), project number(s), task number(s), and work unit number(s). Use the following labels:

C	- Contract	PR	- Project
G	- Grant	TA	- Task
PE	- Program Element	WU	- Work Unit Accession No.

Block 6. Author(s). Name(s) of person(s) responsible for writing the report, performing the research, or credited with the content of the report. If editor or compiler, this should follow the name(s).

Block 7. Performing Organization Name(s) and Address(es). Self-explanatory.

Block 8. Performing Organization Report Number. Enter the unique alphanumeric report number(s) assigned by the organization performing the report.

Block 9. Sponsoring/Monitoring Agency Name(s) and Address(es). Self-explanatory.

Block 10. Sponsoring/Monitoring Agency Report Number. *(If known)*

Block 11. Supplementary Notes. Enter information not included elsewhere such as: Prepared in cooperation with..., Trans. of..., To be published in.... When a report is revised, include a statement whether the new report supersedes or supplements the older report.

Block 12a. Distribution/Availability Statement. Denotes public availability or limitations. Cite any availability to the public. Enter additional limitations or special markings in all capitals (e.g. NOFORN, REL, ITAR).

DOD	-	See DoDD 5230.24, "Distribution Statements on Technical Documents."
DOE	-	See authorities.
NASA	-	See Handbook NHB 2200.2.
NTIS	-	Leave blank.

Block 12b. Distribution Code.

DOD	-	Leave blank.
DOE	-	Enter DOE distribution categories from the Standard Distribution for Unclassified Scientific and Technical Reports.
NASA	-	Leave blank.
NTIS	-	Leave blank.

Block 13. Abstract. Include a brief *(Maximum 200 words)* factual summary of the most significant information contained in the report.

Block 14. Subject Terms. Keywords or phrases identifying major subjects in the report.

Block 15. Number of Pages. Enter the total number of pages.

Block 16. Price Code. Enter appropriate price code *(NTIS only)*.

Blocks 17. - 19. Security Classifications. Self-explanatory. Enter U.S. Security Classification in accordance with U.S. Security Regulations (i.e., UNCLASSIFIED). If form contains classified information, stamp classification on the top and bottom of the page.

Block 20. Limitation of Abstract. This block must be completed to assign a limitation to the abstract. Enter either UL (unlimited) or SAR (same as report). An entry in this block is necessary if the abstract is to be limited. If blank, the abstract is assumed to be unlimited.

FINAL REPORT

Report of Progress on

Soft X-ray Laser Development

submitted to

Air Force Office of Scientific Research

by

Princeton University
Plasma Physics Laboratory
Princeton, New Jersey

October 1988 - October 1989

AFOSR-86-0066

Szymon Suckewer

DESCRIPTION OF RESEARCH PERFORMED IN FY '89

During the past year significant progress was made in generating soft x-ray gain in small scale devices. A critical factor in the application of x-ray lasers to fields such as microscopy and microlithography is the scale and hence cost of the soft x-ray lasers. The collisionally pumped soft x-ray laser in neon-like ions, developed at Livermore[1], requires a large scale laser facility such as Novette or Nova to create a plasma of appropriate conditions. A 3mJ, 182Å soft x-ray laser based on a recombining plasma was developed at Princeton[2] with an efficiency almost 2 orders of magnitude higher than the collisionally pumped case. However the pump laser required, a 30 kJ CO_2 laser, was still large. In order to increase the output energy and efficiency of the 182Å soft x-ray laser we have been developing soft x-ray amplifiers. A gain of $8cm^{-1}$ has been measured in a 3mm long carbon plasma transversely pumped by a 3nsec Nd laser pulse of energy 25J, of which only 15J impinged on the target[3]. We have also demonstrated amplification of 4.5 cm^{-1} in a plasma pumped by only 6J[4] . In this report we present the initial gain measurements at 182Å in a carbon plasma pumped by a 6J laser pulse. We will also present some measurements showing a non-linear rise of intensity with length in an Al plasma pumped by a 6 or 12J laser pulse . We will discuss aspects of data interpretation and gain measurement in such systems.

2. AMPLIFICATION AT 182Å WITH A 6J PUMP LASER

In this section, we present gain measurements on the CVI 182Å transition in a carbon plasma produced with a 6J, 3 nsec Nd:glass laser pulse. The experimental set-up was the same as presented in an earlier paper[4]. Figure 1 shows the rotatable target system used . A 67-cm focal-length spherical lens and 450 cm focal length cylindrical lens were operated in a slightly defocussed arrangement to produce a ~200 μm x 5 mm line-focus on a length-varying cylindrical target. The target lengths used in this experiment were 1, 2.5, and 4.5 mm (limited by the diameter of the access ports in the target chamber). A 0.8 x 2 mm slot in a mask located 1.5 cm away from the target in the axial direction, selected a limited spatial region which was viewed by an axial soft x-ray spectrometer equipped with a multichannel detector. In

the experiments the slot was placed in such a way that it selected a spatial region 0.0 - 0.8 mm from the target surface.

Figure 2 shows the intensity variation of the CV 135Å, OVI 173Å, CVI 182Å, and CV 186Å lines with respect to the plasma length using a 6J, 3 nsec. laser pulse. No stainless steel blade or magnetic field was used. The CVI 182Å line (3-2 transition) increased non-linearly while the CVI 135Å (4-2 transition) and some other lines increased linearly as expected from optically thin spontaneous emission from a homogeneous plasma of length equal to the length of the target. This was a clear indication of gain on the 182Å line. The difference in the length dependence of the 182Å and 135Å lines here is very important (the contribution of the 4th order of the CVI 33.74Å line to 135Å, even for the 1mm plasma, was negligible due to the large opacity of this line). The data were fitted by a nonlinear regression model[5] which performed a least-square fit of the data to the relation:

$$I(L) = \frac{(\exp(GL) - 1)^{3/2}}{(GL \times \exp(GL))^{1/2}} \qquad (1).$$

This describes the output intensity of a Doppler-broadened, homogeneous source of amplified spontaneous emission of gain-length product GL. The fit yielded a value of the gain of 4.5 / cm on the CVI 182Å line and of 0.5 / cm on the CVI 135 Å line (see fig. 3). This result augers well for the commercial availability in the near future of relatively inexpensive soft x-ray lasers for a variety of novel applications.

3. EXPERIMENTS ON ALUMINIUM PLASMAS, ASPECTS OF DATA INTERPRETATION

In the above experiment the plasma length was limited to 4.5mm by the internal diameter of the ports available in the target chamber inside the magnet. A new target chamber was constructed in which plasmas of length of 1cm or more could be produced. This system also had much more flexibility for positioning and angular adjustment of the target and detector (Fig. 4). In this section we present some results from this system showing an non-linear increase of intensity with length of AlX and AlXI lines in an aluminum plasma.

The lithium sequence ions such as AlXI were first used in soft x-ray laser development by Jaeglé and coworkers[6], however the present work on aluminium plasmas pumped with a low energy Nd laser was primarily stimulated by the surprising results of Hara et.al.[7] indicating gain on almost all AlX and AlXI lines observed. It was a simple task to repeat the experiments of Hara et. al. by changing the target material to aluminium.

A Nd glass laser, operated at 6J or 12J, was brought to a line focus by a combination of 4 lenses. Two spherical lenses with a combined focal length of 60cm and two cylindrical lenses produced a sharp line focus 12mm long with a width of 50μm (FWHM) on a rotatable aluminium target with sectors of differing length (2, 6, 10mm) . Axial emission was detected by a soft X-ray multichannel spectrometer "SOXMOS" [8]. SOXMOS was attached to a rotatable arm pivoted under the target so that the angle it viewed could be varied by ± 2° with respect to the target. The target assembly was on a platform that could be rotated ±2° around a vertical axis so that by combining the two motions, emission over a ±4° axial range in the horizontal plane could be recorded. This system was designed to allow the most precise alignment of the target with respect to the spectrometer and also enable the detection of a stimulated soft X-ray beam that had been deviated from the nominal axial direction by refraction in the plasma. A slot with open area 3mm high and 0.35mm wide was placed on axis 4 cm from the target to limit the view of the spectrometer. The position of the slot could be adjusted to view regions of the plasma at different distances from the target surface.

In the experiment a search for gain was performed by varying the experimental parameters (including the target length) and looking for conditions in which the intensity of candidate lines increased with length at a rate that was faster than linear. A faster-than-linear rise of intensity with length is commonly regarded as conclusive evidence for stimulated emission.

Figure 5 shows axial spectra of AlIV, OVI, AlX, and AlXI lines at 2mm and 10mm target lengths. A dramatic increase of intensity of the AlX and AlXI lines is seen with the 10mm target as compared to 2mm, while the AlIV and OVI lines show a sub-linear increase. Figure 6 shows peak intensities taken at 2, 6, and 10mm target lengths and a curve fit to the data. The theoretical fit was derived from a nonlinear regression model[6] as in the CVI case. In general the transition linewidth will be a convolution of Stark and Doppler broadening but

for the present purposes we have used the gain equation based on the Doppler broadening.

A higher laser energy was used in order to increase the output intensity. Data taken at 12J is shown in Figs. 7 and 8. Here the increase with length is even more dramatic, for instance the AlXI 141Å (3s-4p) intensity increases from 2mm to 10mm by a factor of x50 and is an excellent fit to the gain equation for a gain of G = 5.1/cm. The AlXI 150Å (3p-4d), 154Å (3d-4f) and AlX 177Å (3d-4f) lines also show a length dependence which is a very close fit to the gain equation at comparable values of gain. Similar results were obtained for the AlXI 105.7Å (3d-5f) and 103.8Å (5d-3p) lines.

The emission from the plasma was recorded on a time-resolving streaked spectrometer[9], " TGSS " placed on-axis, on the opposite side of the plasma to the spectrometer: SOXMOS . A free standing gold transmission grating with a 3000Å period and 250μm entrance slit, dispersed the axial plasma emission along the entrance slit of an x-ray streak camera. The entrance slit was 12mm long, 1mm wide, and coated with a 200Å thick aluminium photocathode. This grating, streak camera arrangement resulted in a source-size-limited spectral resolution for these experiments of approximately 3Å. The spectral range of the instrument extended from 110Å to 190Å.

The streaked image was amplified by an image intensifier and recorded on calibrated TriX film placed in contact with the output of the image intensifier. The sweep speed was 1.25nsec/mm resulting in a temporal resolution of approximately 0.25nsec. Figure 9 shows detailed time histories of the 154Å and 162Å emission taken with 12J of laser energy. The emission had a total duration of 6nsec.

Data Analysis

There are some unexpected features to the data in Figs 5-8. First of all, every AlX and AlXI line observed, without exception, showed a non-linear increase with length. In general the gain coefficient depends on the factors shown in equation 2:

$$G = \frac{1}{8\pi c}\,\frac{\lambda^4}{\Delta\lambda}\; g_i A_{ik} \left\{ \frac{N_i}{g_i} - \frac{N_k}{g_k} \right\} \qquad (2).$$

Here G is the gain coefficient, and λ the wavelength. g is the statistical weight, A_{ik} the radiative transition probability and N the population of the upper level i and lower level k. The highest gain was expected on the 3-4 transition with the largest gA value (3d-4f at 154Å), however the data shows high gain on all the AlXI and AlX lines observed, similarly to reference 8. Particularly surprising was the strong increase apparent on the AlXI 141Å line. which has a gA value much lower than the 150Å and 154Å transitions. The time history observed with the streak camera showed no difference between the time evolution at 154Å and the continuum background at 162Å (Figure 9). Another unexpected feature is the large rise in the background continuum emission, from 5-10 counts at 2mm to ~200 counts at 10mm. These features raised concerns about the homogeneity of the plasma along its length . Specifically, were the level populations in the region of the 2mm plasma viewed by the spectrometer identical to the conditions in the 10 mm section? As shown in Fig. 4, the 2, 6 and 10mm sections shared a common boundary on the spectrometer end of the target wheel. To test if the plasma was homogeneous a target was built with the 2mm sections on both ends of the target and the 6mm section on the end of the target away from the spectrometer. First the conditions were arranged so as to reproduce the previous 10mm spectra and then the emission from the two 2mm sections at each end of the target was compared. It was immediately apparent that there was a large difference in intensity between the 2mm section at the spectrometer end and the 2mm section at the opposite end. Taking the average of the 2mm results, the best fit to the data was now a linear increase in intensity with length as shown in Fig. 10. The reason for the non-uniformity lay in a small angle between the target surface and the region viewed by the spectrometer (Fig. 11), possibly caused by refraction. To verify this, the target was rotated about a vertical axis to change the position of the plasma generated by the two 2mm sections with respect to the region viewed by the spectrometer. With a 2° rotation the AlXI 154Å emission from the two ends became equal. In this configuration however the length dependance of the emission was linear. In conclusion; the non-linear increase in Figs 5-8 was caused by geometrical effects and *not* by stimulated emission.

As noted before the measurement of an exponential intensity increase with length is commonly regarded as conclusive evidence for gain (see for instance ref 9). However in view of the above results it is clear that while this

may be an encouraging sign of gain it is by no means sufficient proof that gain is present. As was done in some earlier works (for example references 2, 4, 7, 10), it is critical to monitor the emission from nearby spontaneous emission lines in the same ion, preferably lines with the same lower level as the lasing line, to be assured that one is viewing a homogeneous plasma and that the comparison of plasmas of differing lengths is a valid. This is particularly important for measurements of low gain-lengths, GL $\leq$ 4, where the enhancement of stimulated as compared to spontaneous emission is less that an order of magnitude.

Figure Captions

Fig. 1 The rotatable target system.

Fig. 2 Spectra obtained with 6J laser energy from carbon plasmas of length: (a) 1mm, (b) 2.5mm and (c) 4.5 mm .

Fig. 3 Intensities of the CVI 182Å and CVI 135Å lines versus plasma length and (dashed line) a least squares fit to the gain equation (eqn. 1) with a gain of 4.5 cm^{-1} for the 182Å line.

Fig. 4 Improved experimental set-up for gain measurements showing the range of angular adjustments available.

Fig. 5 Aluminum spectra obtained at **6J** laser energy with target lengths 2mm and 10mm.

Fig. 6 Dependence of the AlXI 154Å and AlX 177Å axial line intensity on length. The line represents a fit of the experimental points to the theoretical gain equation (eqn. 1 in the text).

Fig. 7 Spectra obtained at **12J** laser energy with target lengths 2mm and 10mm. Note the x10 scale change from the 2mm to 10mm graph.

Fig. 8 Dependence of the AlXI 141Å, 150Å,154Å and AlX 177Å axial line intensity on length. The line represents a theoretical fit of the experimental points to the gain equation (eqn. 1 in the text).

Fig. 9 Detailed time histories of (a) 154Å and (b) 162Å emission taken with 12J of laser energy. The fluctuations are caused by film grain.

Fig. 10 (a) data showing the 154Å intensity variation with length but in this case including 2mm sections from both ends of the target. The 6mm data was from a section at the opposite end of the target to the data in Figs 5-8. (b) as above but with the target rotated by 2°.

Fig. 11 Illustration of the effect of a small angle between the plasma and the region viewed by the spectrometer. The comparison of plasmas of differing lengths cannot be used for measurements of gain in this case.

References

1 D. L. Matthews, P. L. Hagelstein, M. D. Rosen, M.J. Eckart, N.M. Ceglio, A. U. Hazi, J. Medecki, B. J. MacGowan, J. E. Trebes, B. L. Whitten, E. M. Campbell, C. W. Hatcher, A. M. Hawryluk, R. L. Kaufman, L. D. Pleasance, G. Rambach, J. Scofield, G. Stone, and T. A. Weaver, *Phys. Rev. Lett.* **54,** 110, (1985) and C.J.Keane, N.M.Ceglio, B. J. MacGowan, D. L. Matthews, D. G. Nilson, J. E. Trebes, and D. A. Wilson *J. Phys. B.* **22**, 3343, (1989).

2 S. Suckewer, C. H. Skinner, D. Kim, E. Valeo, D. Voorhees, and A. Wouters *Phys Rev. Lett.* **57**, 1004, (1986).

3 D.Kim, C.H. Skinner, G. Umesh, and S. Suckewer *Optics Letters*, **14**, 665-667, 1989.

4 S. Suckewer X-ray laser Related Experiments and Theory at Princeton *OSA Proceedings on Short Wavelength Coherent Radiation: Generation and Applications* **2,** 36, (1988).

5 based on the RNLIN subroutine in the IMSL STAT/LIBRARY p239.

6 G. Jamelot, P. Jaeglé, A. Carillon, F. Gadi, B. Gauthé, H. Guennou, A. Klisnick, C. Möller, and A. Sureau, *I.E.E.E. Trans on Plasma Science,* **16**, 497, (1988).

7 T. Hara, K. Ando, N. Kusakbe, H. Yashiro, and Y. Aoyagi *Jpn. J of Appl. Phys.* **6**, 1010-1012, (1989).

8 J.L.Schwob, A. Wouters, and S. Suckewer, *Rev. Sci. Instrum.* 58, 1601, (1987).

9 N.M.Ceglio in *Laser Interaction and Related Phenomena*, H. Hora and G. Miley,eds., **7**, 39, Plenum Press, New York, 1986. In the present work the TGSS was used without the imaging mirror described in this reference.

10 S. Suckewer, C. H. Skinner, D. Kim, E. Valeo, D. Voorhees, and A. Wouters *Phys Rev. Lett.* **57**, 1004, (1986) and D. Kim, C. H. Skinner, A. Wouters, E. Valeo, D. Voorhees and S. Suckewer *J. Opt. Soc Am B* **6**, 115, 1989.

Figure Captions

Fig. 1a The Target Chamber used to generate a gain of 4.5 cm^{-1} at 182Å. Its size is 3" x 3" x 6" .

Fig. 1b Schematic of the rotatable target system.

Fig. 2 Spectra obtained with 6J laser energy from carbon plasmas of length: (a) 1mm, (b) 2.5mm and (c) 4.5 mm .

Fig. 3 Intensities of the CVI 182Å and CVI 135Å lines versus plasma length and (dashed line) a least squares fit to the gain equation (eqn. 1) with a gain of 4.5 cm^{-1} for the 182Å line.

Fig 4 Improved experimental set-up for gain measurements showing the range of angular adjustments available.

Fig. 5 Aluminum spectra obtained at **6J** laser energy with target lengths 2mm and 10mm.

Fig. 6 Dependence of the AlXI 154Å and AlX 177Å axial line intensity on length. The line represents a fit of the experimental points to the theoretical gain equation (eqn. 1 in the text).

Fig. 7 Spectra obtained at **12J** laser energy with target lengths 2mm and 10mm. Note the x10 scale change from the 2mm to 10mm graph.

Fig. 8 Dependence of the AlXI 141Å, 150Å,154Å and AlX 177Å axial line intensity on length. The line represents a theoretical fit of the experimental points to the gain equation (eqn. 1 in the text).

Fig. 9 Detailed time histories of (a) 154Å and (b) 162Å emission taken with 12J of laser energy. The fluctuations are caused by film grain.

Fig. 10 (a) data showing the 154Å intensity variation with length but in this case including 2mm sections from both ends of the target. The 6mm data was from a section at the opposite end of the target to the data in Figs 5-8. (b) as above but with the target rotated by 2°.

Fig. 11 Illustration of the effect of a small angle between the plasma and the region viewed by the spectrometer. The comparison of plasmas of differing lengths cannot be used for measurements of gain in this case.

References

1 C.J.Keane et al., *J. Phys. B.* **22**, 3343, (1989).

2 S. Suckewer, C. H. Skinner, D. Kim, E. Valeo, D. Voorhees, and A. Wouters *Phys Rev. Lett.* **57**, 1004, (1986).

3 D.Kim, C.H. Skinner, G. Umesh, and S. Suckewer *Optics Letters*, **14**, 665-667, 1989.

4 S. Suckewer X-ray laser Related Experiments and Theory at Princeton *OSA Proceedings on Short Wavelength Coherent Radiation: Generation and Applications* **2**, 36, (1988).

5 . ..sed on the RNLIN subroutine in the IMSL STAT/LIBRARY p239.

6 G. Jamelot, P. Jaeglé, A. Carillon, F. Gadi, B. Gauthé, H. Guennou, A. Klisnick, C. Möller, and A. Sureau, *I.E.E.E. Trans on Plasma Science*, **16**, 497, (1988).

7 T. Hara, K. Ando, N. Kusakbe, H. Yashiro, and Y. Aoyagi *Jpn. J of Appl. Phys.* **6**, 1010-1012, (1989).

8 J.L.Schwob, A. Wouters, and S. Suckewer, *Rev. Sci. Instrum.* 58, 1601, (1987).

9 N.M.Ceglio in *Laser Interaction and Related Phenomena*, H. Hora and G. Miley,eds., **7**, 39, Plenum Press, New York, 1986. In the present work the TGSS was used without the imaging mirror described in this reference.

10 S. Suckewer, C. H. Skinner, D. Kim, E. Valeo, D. Voorhees, and A. Wouters *Phys Rev. Lett.* **57**, 1004, (1986) and D. Kim, C. H. Skinner, A. Wouters, E. Valeo, D. Voorhees and S. Suckewer *J. Opt. Soc. Am B* **6**, 115, 1989.

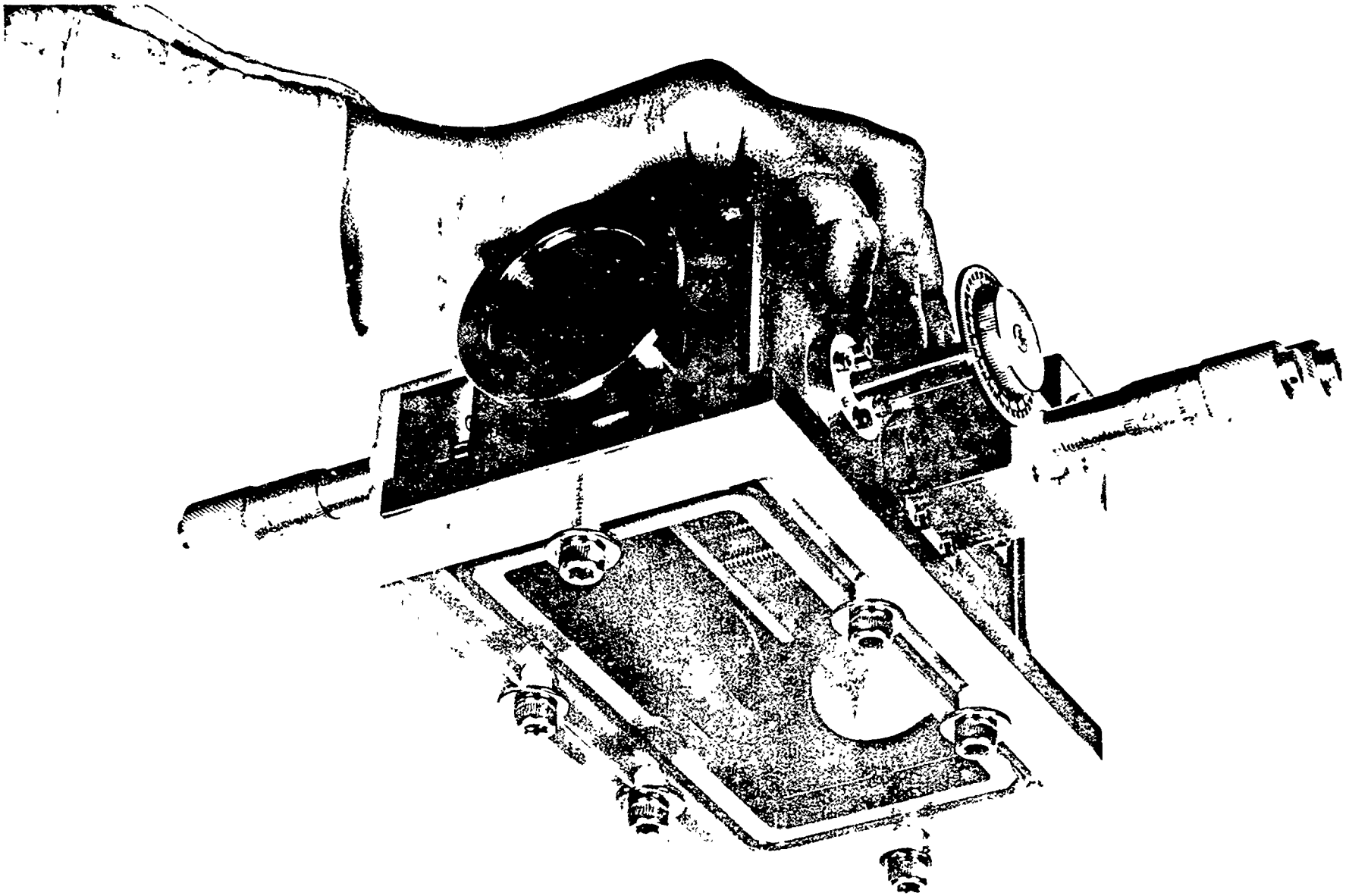

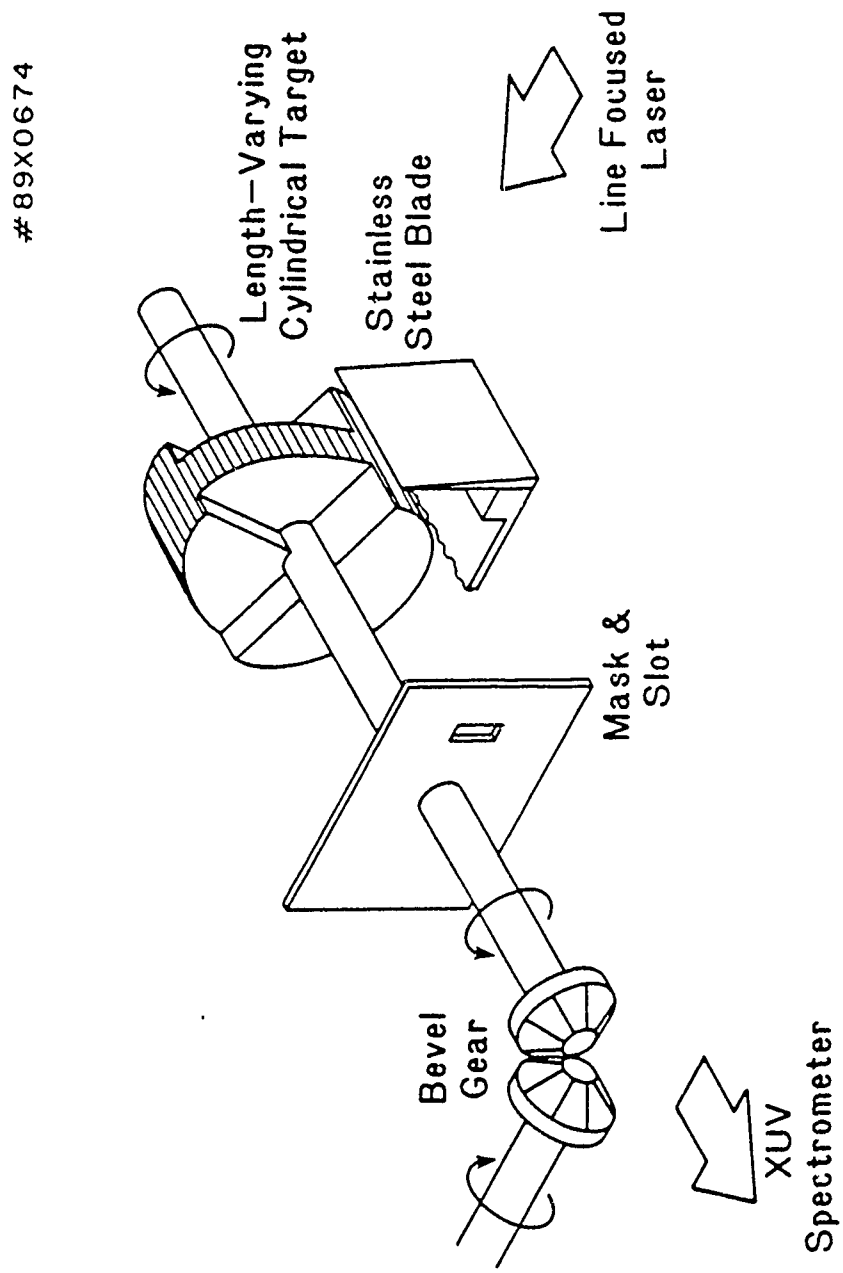
#89X0674
Length–Varying
Cylindrical Target
Stainless
Steel Blade
Line Focused
Laser
Mask &
Slot
Bevel
Gear
XUV
Spectrometer

Fig. 1b

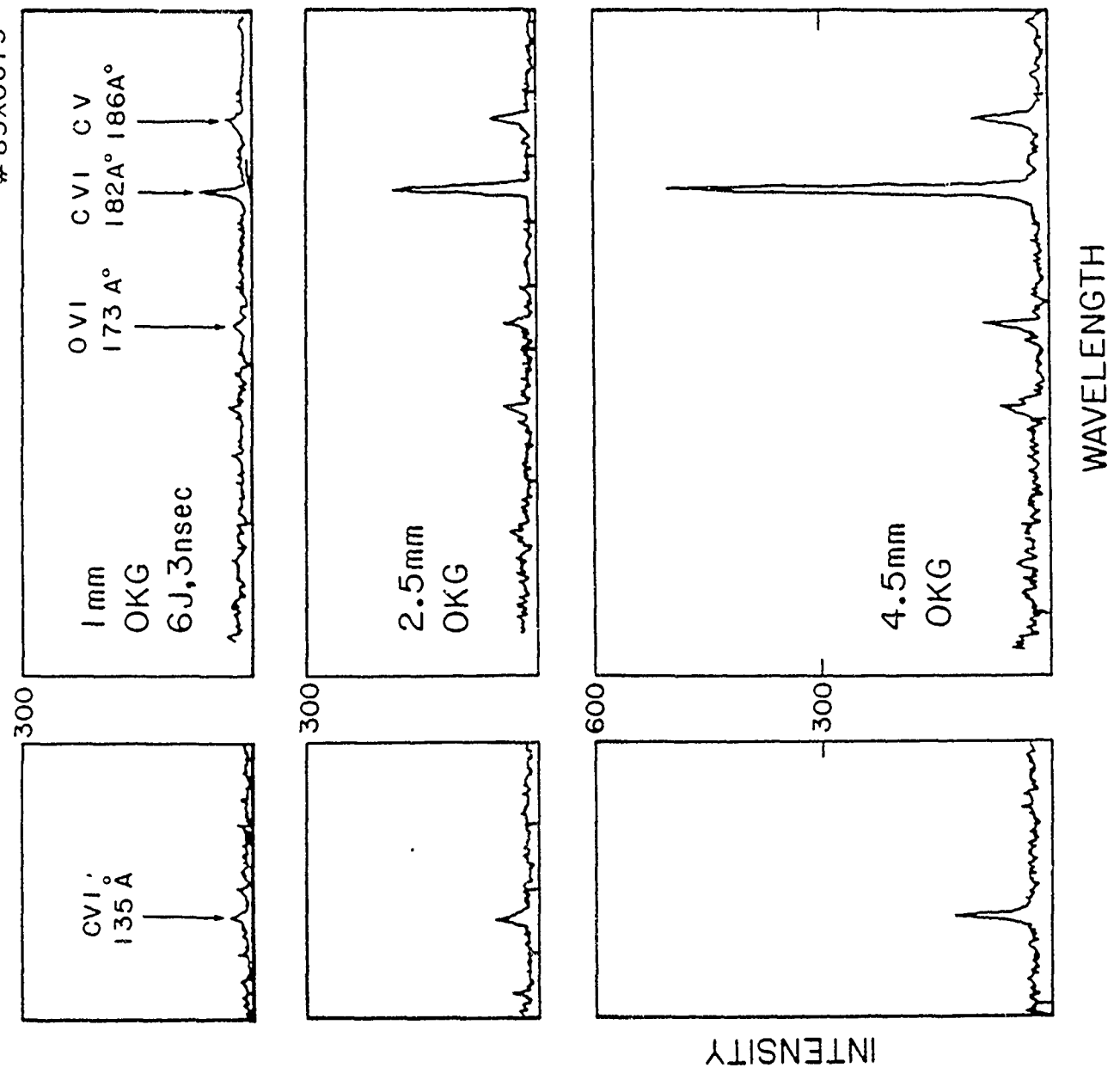
#89X0675
300
CVI
135 Å
1mm
OKG
6J,3nsec
OVI
173 A°
CVI CV
182A° 186A°
300
2.5mm
OKG
600
300
4.5mm
OKG
INTENSITY
WAVELENGTH

Fig. 2

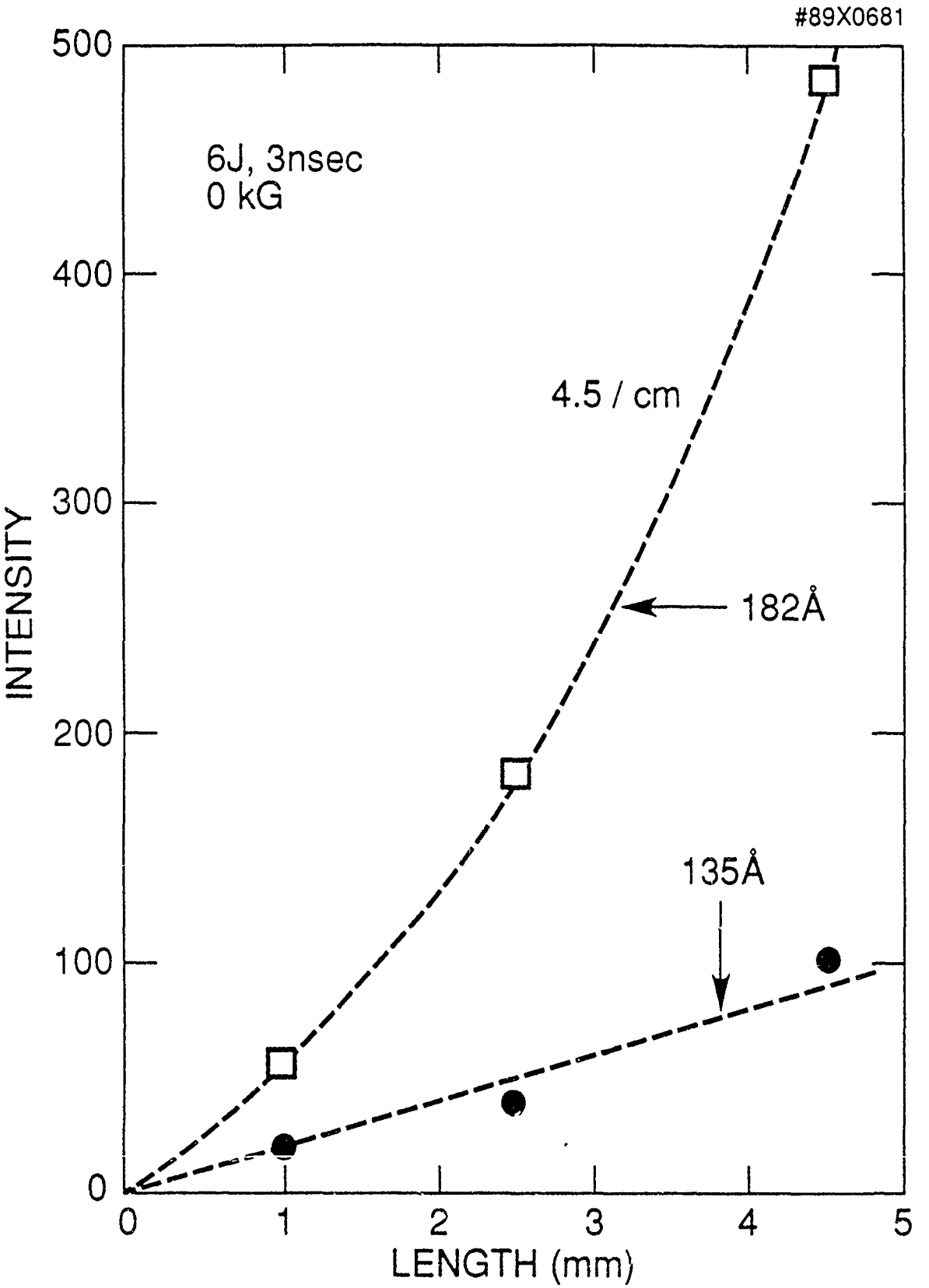
#89X0681
6J, 3nsec
0 kG
4.5 / cm
182Å
135Å
INTENSITY
LENGTH (mm)
500
400
300
200
100
0
0
1
2
3
4
5

Fig. 3

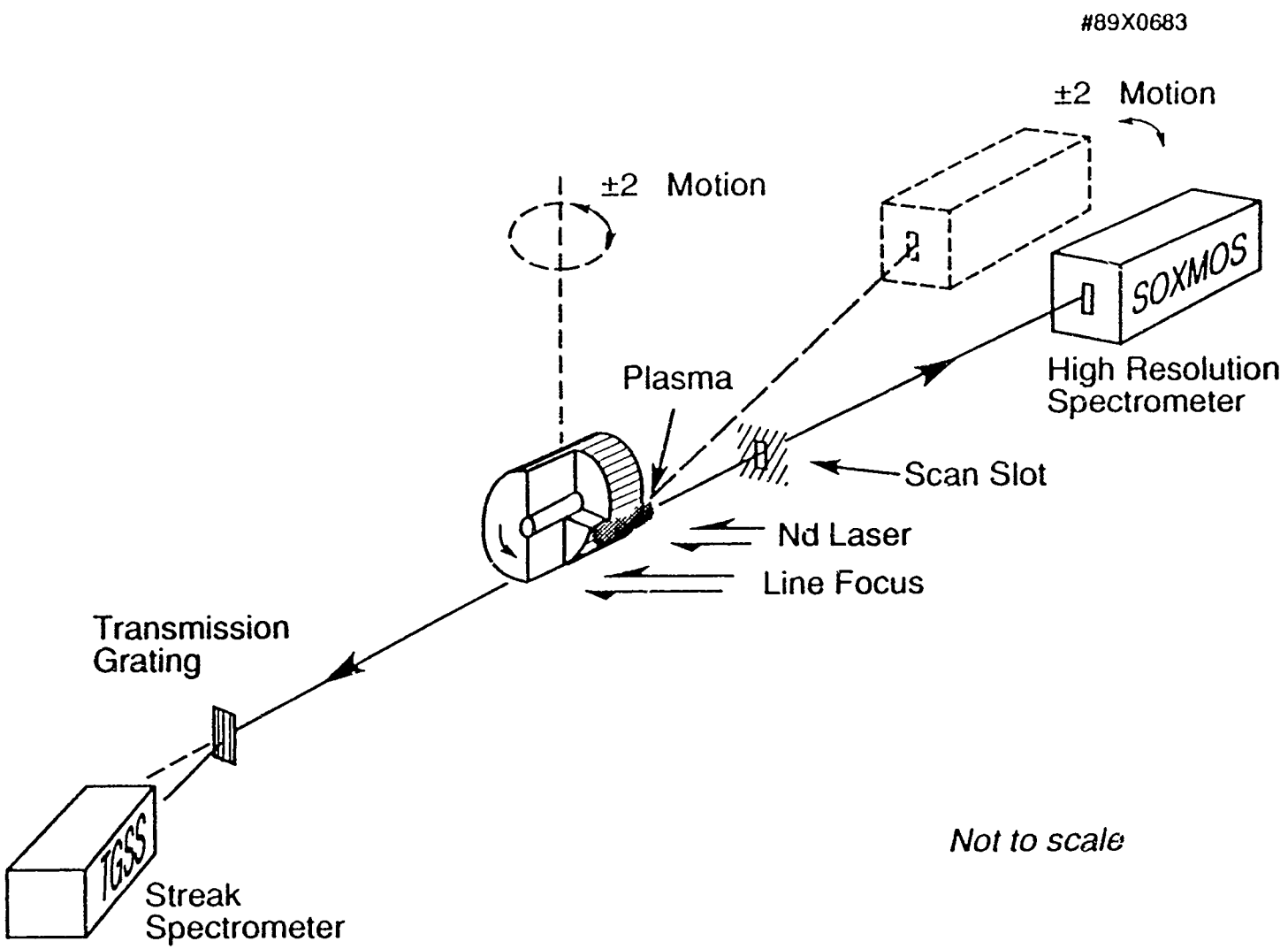
#89X0683
±2 Motion
±2 Motion
SOXMOS
High Resolution
Spectrometer
Plasma
Scan Slot
Nd Laser
Line Focus
Transmission
Grating
TGSS
Streak
Spectrometer
Not to scale

Fig. 4

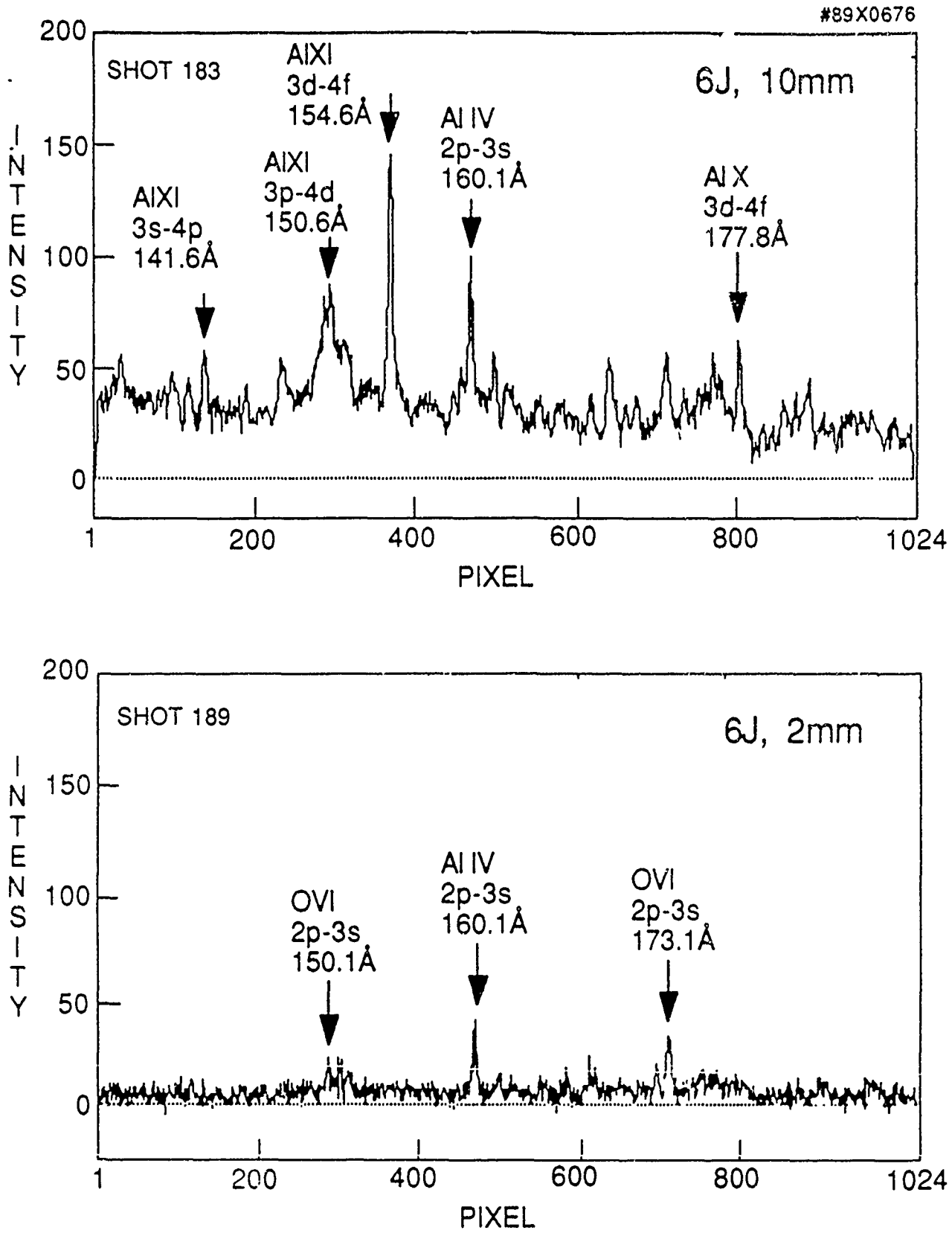
#89X0676
SHOT 183
6J, 10mm
AlXI
3d-4f
154.6Å
Al IV
2p-3s
160.1Å
AlXI
3p-4d
150.6Å
AlXI
3s-4p
141.6Å
Al X
3d-4f
177.8Å
INTENSITY
200
150
100
50
0
1
200
400
600
800
1024
PIXEL
SHOT 189
6J, 2mm
OVI
2p-3s
150.1Å
Al IV
2p-3s
160.1Å
OVI
2p-3s
173.1Å
INTENSITY
200
150
100
50
0
1
200
400
600
800
1024
PIXEL

Fig. 5

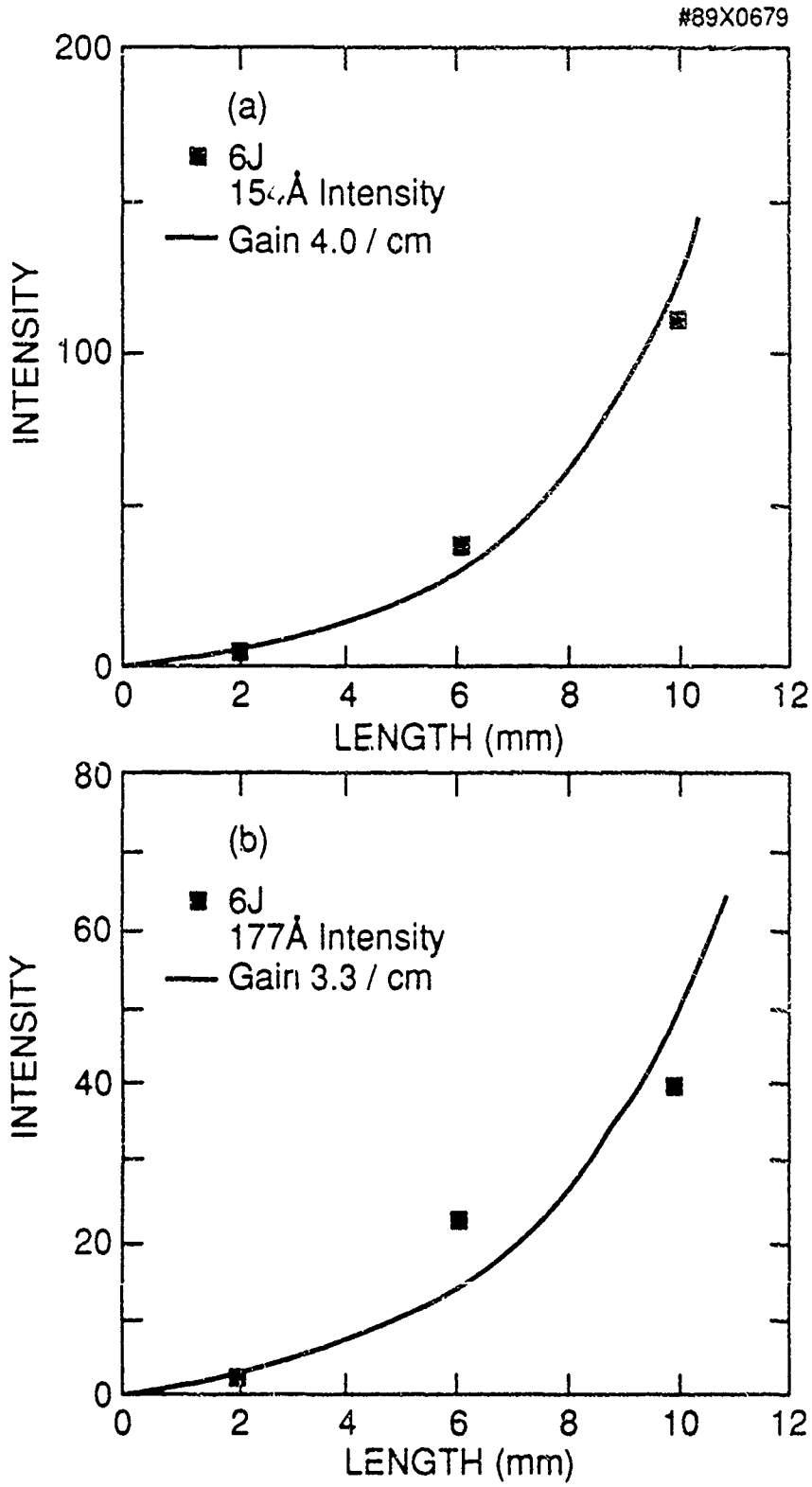
#89X0679
200
100
0
INTENSITY
(a)
6J
154Å Intensity
Gain 4.0 / cm
0
2
4
6
8
10
12
LENGTH (mm)
80
60
40
20
0
INTENSITY
(b)
6J
177Å Intensity
Gain 3.3 / cm
0
2
4
6
8
10
12
LENGTH (mm)

Fig. 6

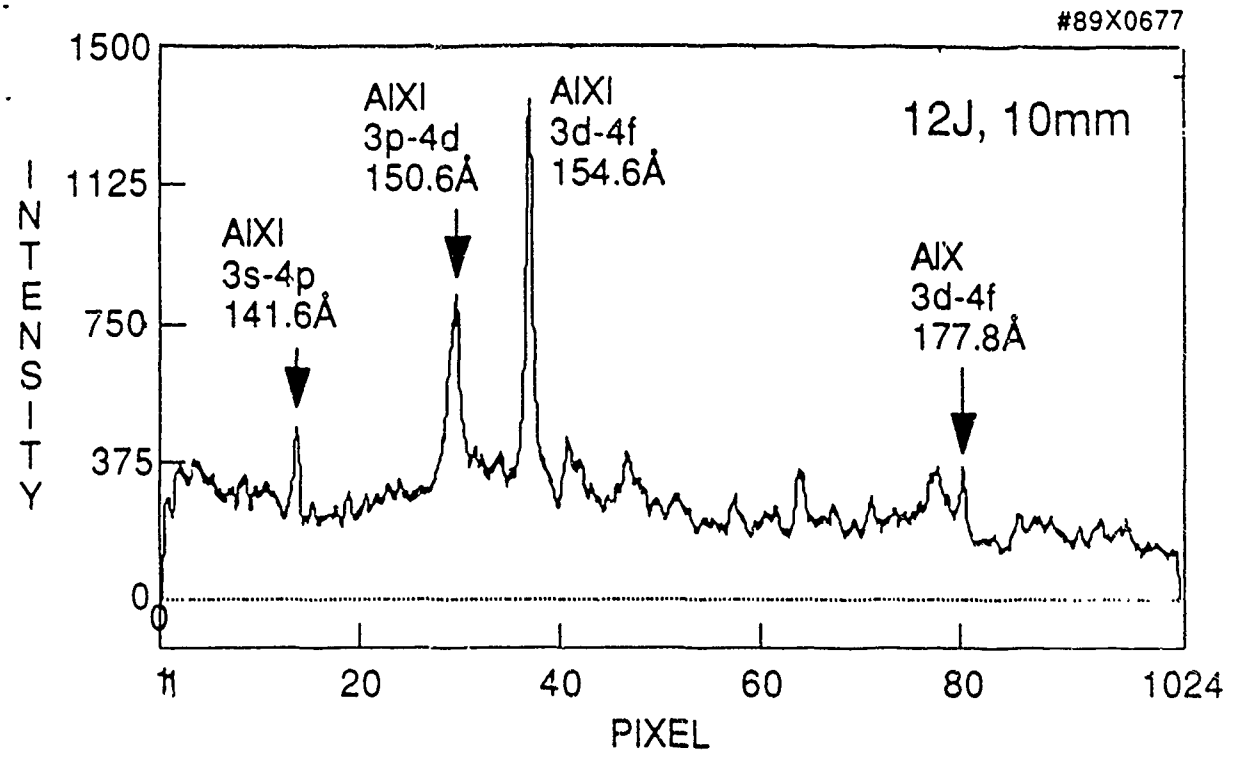
#89X0677
1500
1125
750
375
0
INTENSITY
AlXI
3s-4p
141.6Å
AlXI
3p-4d
150.6Å
AlXI
3d-4f
154.6Å
12J, 10mm
AlX
3d-4f
177.8Å
1
20
40
60
80
1024
PIXEL

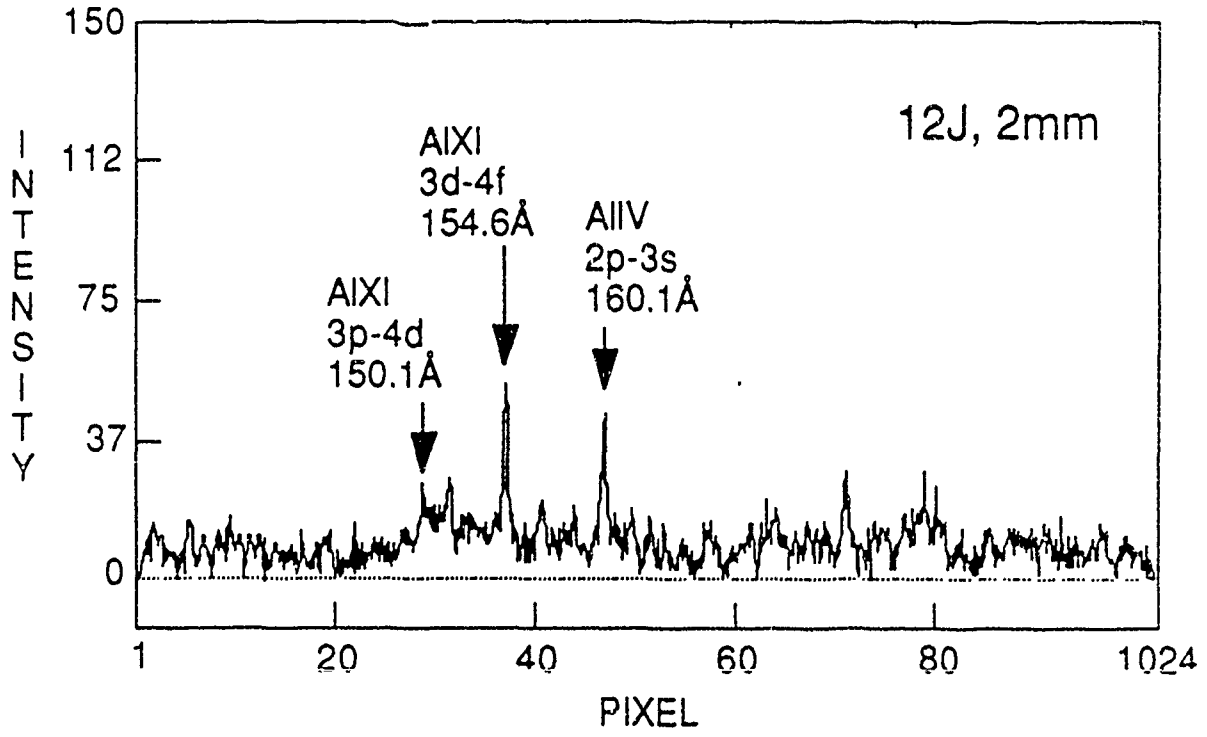
150
112
75
37
0
INTENSITY
AlXI
3d-4f
154.6Å
AlIV
2p-3s
160.1Å
AlXI
3p-4d
150.1Å
12J, 2mm
1
20
40
60
80
1024
PIXEL

Fig. 7

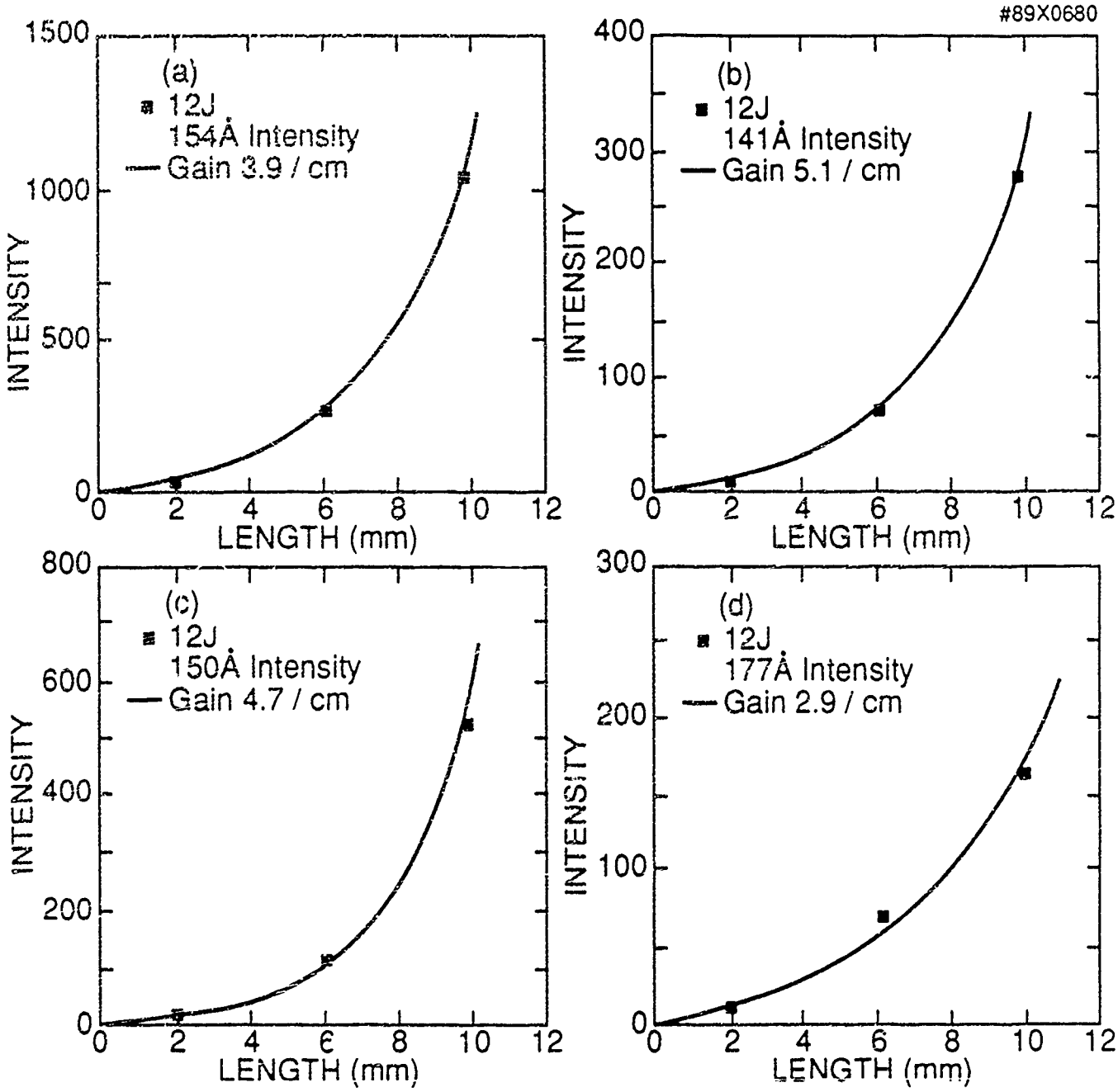
#89X0680
(a)
12J
154Å Intensity
Gain 3.9 / cm
INTENSITY
LENGTH (mm)
(b)
12J
141Å Intensity
Gain 5.1 / cm
INTENSITY
LENGTH (mm)
(c)
12J
150Å Intensity
Gain 4.7 / cm
INTENSITY
LENGTH (mm)
(d)
12J
177Å Intensity
Gain 2.9 / cm
INTENSITY
LENGTH (mm)

Fig. 8

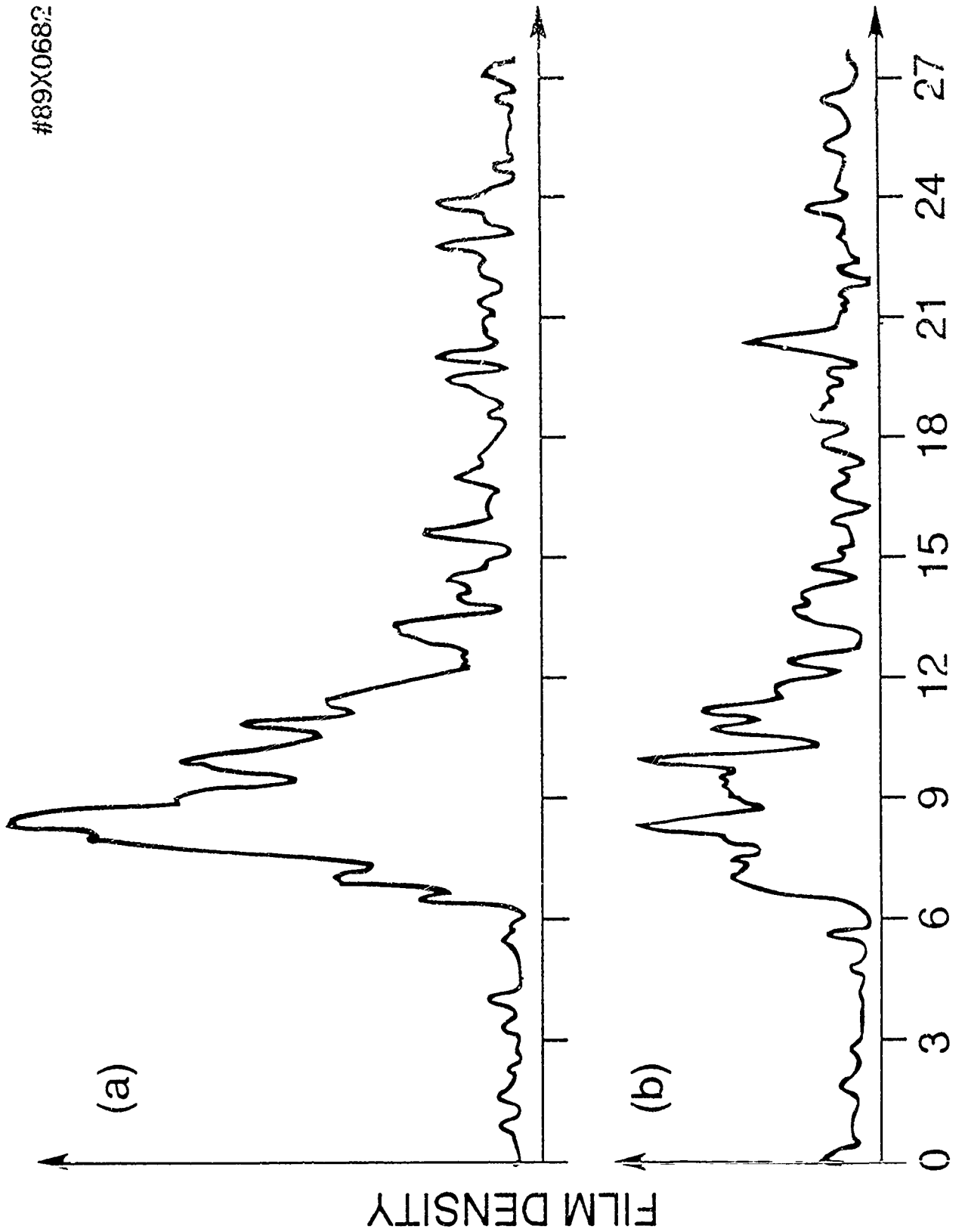

Fig. 9

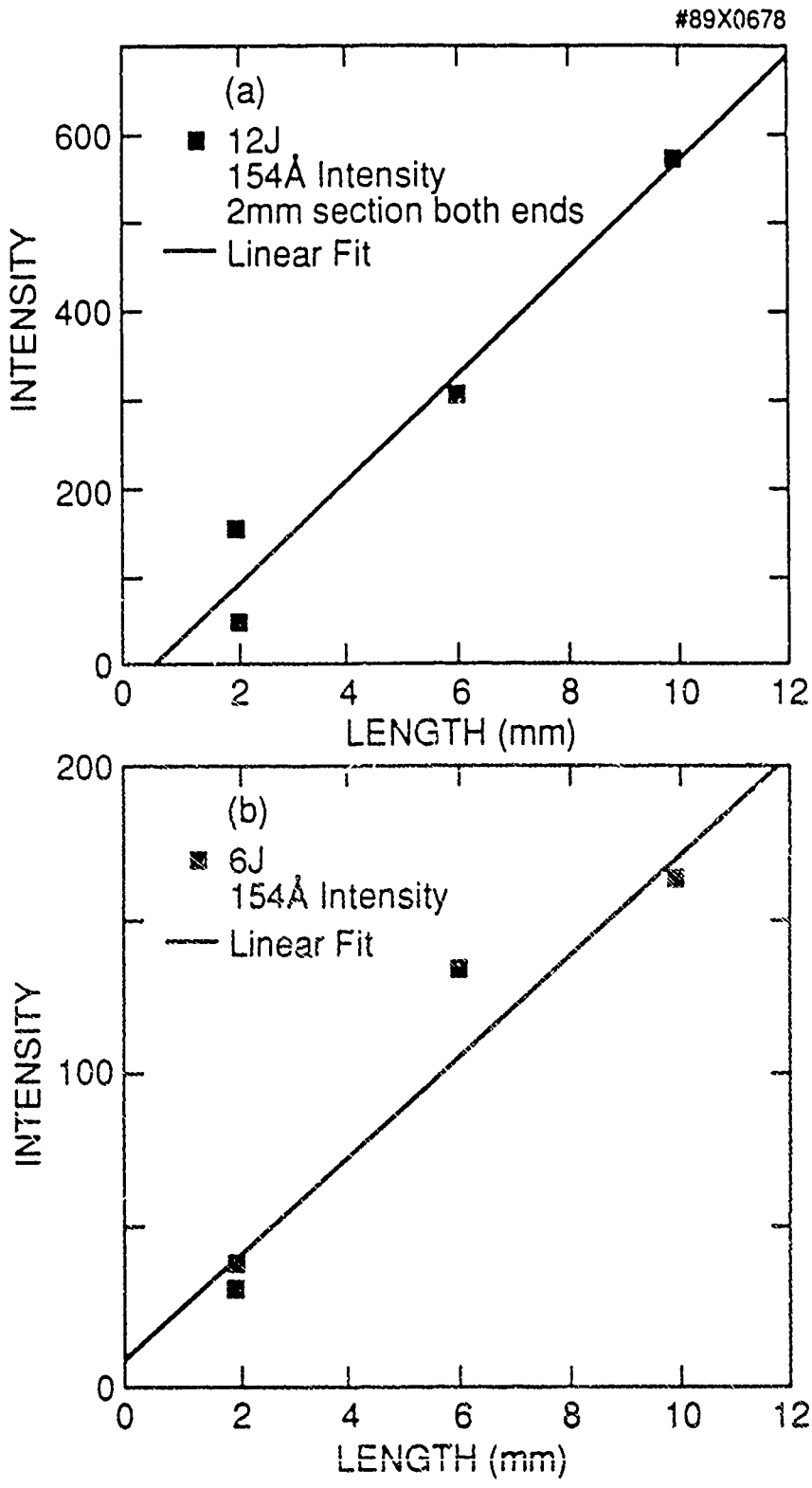
#89X0678
(a)
12J
154Å Intensity
2mm section both ends
Linear Fit
INTENSITY
600
400
200
0
0
2
4
6
8
10
12
LENGTH (mm)
(b)
6J
154Å Intensity
Linear Fit
INTENSITY
200
100
0
0
2
4
6
8
10
12
LENGTH (mm)

Fig. 10

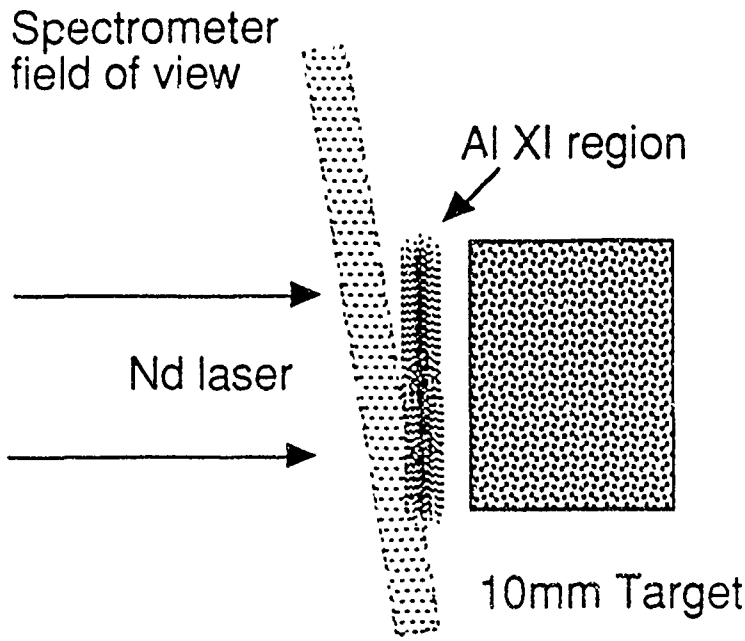
Spectrometer
field of view
Al XI region
Nd laser
10mm Target

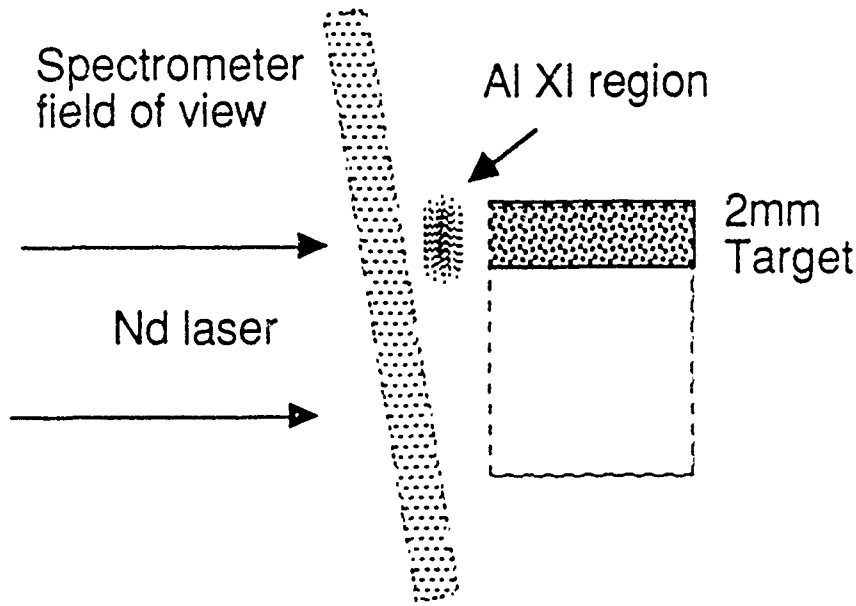
Spectrometer
field of view
Al XI region
2mm
Target
Nd laser

Fig. 11

Gain measurements at 18.22 nm in C VI generated by a Nd:glass laser

D. Kim, C. H. Skinner, G. Umesh, and S. Suckewer

a reprint from Optics Letters

Gain measurements at 18.22 nm in C VI generated by a Nd:glass laser

D. Kim, C. H. Skinner, G. Umesh, and S. Suckewer

Princeton Plasma Physics Laboratory, Princeton University, Princeton, New Jersey 08543

Received September 19, 1988; accepted April 11, 1989

We present recent gain measurements in C VI at 18.22 nm for a soft-x-ray amplifier produced by a line-focused glass laser (1.053 μm) on a solid carbon target. The maximum gain measured was 8 ± 2 cm^{-1} in the recombining plasma column, with additional radiation cooling by iron impurities.

Recent research in soft-x-ray laser development is progressing in the direction of obtaining shorter wavelengths. Significant advances are also being made in the XUV region. Much attention is being devoted to the first applications of these lasers. The possibility of using soft-x-ray lasers for the microscopy of living cells has stimulated research in the development of x-ray lasers operating in the wavelength region of 2.33–4.37 nm, the so-called water window.[1,2] Impressive advances in longer-wavelength XUV lasers, such as the one recently demonstrated at 108.9 nm,[3,4] have significant potential applications in chemistry. An important point, however, that is rarely discussed is the laser energy required for these applications. For example, in order to record a high-resolution image of a biological cell on a photoresist, substantial laser beam energy is required. This is a significant concern in our current soft-x-ray microscopy experiments,[5] even for the maximum output energy of our current 18.22-nm laser.[6]

We have, therefore, applied a significant effort to increase the energy of the 18.22-nm soft-x-ray laser. One approach has been to develop additional amplifiers. This technique can also be applied to the shorter-wavelength region, where our current goals include the generation of lasing action near 10.0 nm, using ions in the Li-like sequence,[7] and down to 1.0 nm, using a powerful picosecond laser for selective excitation.[8]

In this Letter we present the first step in developing such amplifiers by the generation of gain in C VI at 18.22 nm using a Nd:glass laser beam brought to a line focus on a solid carbon target in a strong magnetic field (field lines parallel to the line focus). The role of the magnetic field is considered to be less important here than in our research in generating gain at 18.22 nm using a CO_2 laser that is point focused along the magnetic-field axis because of a much higher initial electron density for the 1-μm Nd:glass laser than for the 10-μm CO_2 laser. However, in the future we plan to combine this amplifier with our CO_2-laser-pumped, magnetically confined soft-x-ray laser; thus it is necessary that the Nd:glass-laser-pumped amplifier also work in a magnetic field and have a similar transverse dimension.

In the experiments the maximum pumping laser energy used was 40 J, which was limited by the area of the beam input optics, and the pulse duration was 3 nsec. The 5.1-cm-diameter laser beam was line focused onto the cylindrical target by the combination of a 67-cm focal-length spherical lens and a 450-cm focal-length cylindrical lens (Fig. 1). The dimensions of the line focus were ~100 μm × 5 mm. The length of the line focus was limited by the size of the magnet port. One of the features of the target system was the capability of rotating the target so that for every shot a fresh target surface is exposed by the laser. A similar condition was created in the experiments performed by Jaeglé *et al.*[9] by translation of a plane aluminum target. The gain was measured by changing the target length and hence the plasma length, as shown in Fig. 1.

Another feature was a stainless-steel blade in front of the target. The 0.25-mm-thick stainless-steel blade was placed 0.8 mm from the target surface. The function of the blade was to provide an additional cooling source: fully stripped carbon ions in the laser-produced plasma interact with the blade and cool rapidly through thermal conduction and line radiation. The concept of conductive cooling by a metal plate was first suggested by Bhagavatula and Yaakobi.[10]

Experiments with a target without the stainless-steel blade showed significantly lower gain: with 32 J

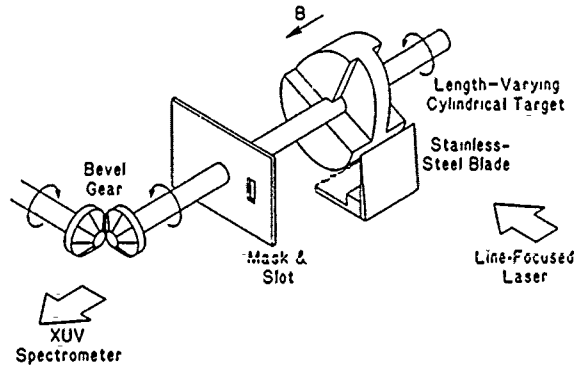

Fig. 1. The rotatable-target system. B, An axial magnetic field.

0146-9592/89/130665-03$2.00/0

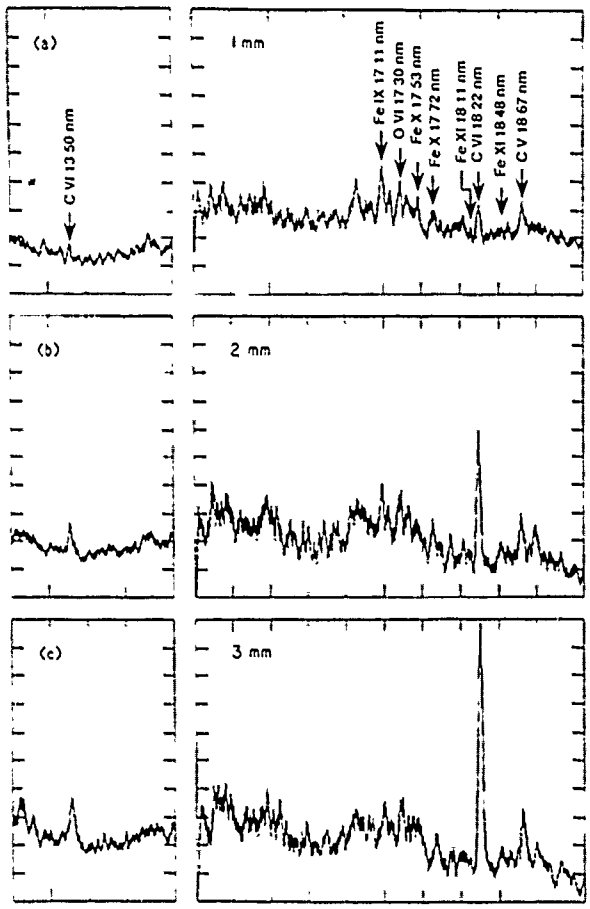

Fig. 2. Experimental spectra obtained by a XUV spectrometer for plasma lengths of (a) 1 mm, (b) 2 mm, and (c) 3 mm with 25 J of laser energy and a magnetic-field strength of 50 kG.

of laser energy a gain of 4.5 cm^{-1} was measured with the blade, compared with 0.4–0.8 cm^{-1} without the blade. A limited spatial region is selected by a slot in a mask 1.5 cm from the target in the axial direction and viewed by a soft-x-ray spectrometer located 2.6 m from the target in the axial direction. For the data presented below the slot size was 0.8 mm × 2 mm, and the near edge of the slot was 0.5 mm from the target surface. Hence the region selected by the slot included an area surrounding the blade.

Experiments in which the radial distance from the edge of the slot to the target was varied indicated that C VI was abundant in the region 0–2 mm from the target surface. The region selected by the slot for the gain measurements (0.5–1.3 mm from the target surface) was judged to have the most favorable conditions for gain.

Figure 2 shows the experimental data recorded with an axial-grazing-incidence soft-x-ray spectrometer. The angle of incidence was 88°, and the intensities of multiple orders were negligible. It was equipped with a 1200-groove/mm grating at a blaze angle of 1° and a multichannel detector. The intensity dependences of the C VI 13.50-nm, C VI 18.22-nm, and C V 18.67-nm lines with respect to plasma length are shown. The data were obtained with 25 J of laser energy and the stainless-steel blade and slot dimensions as described above. The magnetic field was 50 kG. In the experiments we found that the variation of laser intensity over the line focus limited the length of the plasma over which gain could be achieved, to approximately 3 mm. Attempts to create a uniform plasma longer than 3 mm showed that a C VI 13.50-nm intensity increased less than linearly. This indicated that the weaker laser intensity beyond the central 3-mm-long region did not create the same plasma conditions as in the central region. For the gain measurements plasma lengths of 1, 2, and 3 mm were used, and the plasma uniformity is evidenced by the linear increase of the C VI 13.50-nm intensity with length. Emission by iron is clearly seen in the spectra. The 18.22-nm line from C VI is blended with a line of similar wavelength from Fe XI 18.22 nm. Without correction for contamination due to Fe XI 18.22 nm, the estimated gain is $5 \pm 2\ cm^{-1}$. The line intensity of Fe XI 18.22 nm is known to be approximately the same as those of Fe XI 18.11 and 18.48 nm.[11] Since the Fe XI 18.11-, 18.22-, and 18.48-nm lines originate from the same $3p^3 3d$ upper level, the use of line intensity ratios in Ref. 11 provides a reasonable approximation in estimating the contribution of Fe XI 18.22 nm. The average of the line intensities of Fe XI 18.11 and 18.48 nm is used in correcting the line intensity of C VI 18.22 nm. In Fig. 3 the corrected line intensities of C VI 18.22 nm (integrated over time and frequency) are plotted versus the plasma length. The data have been fitted by the relation[12]

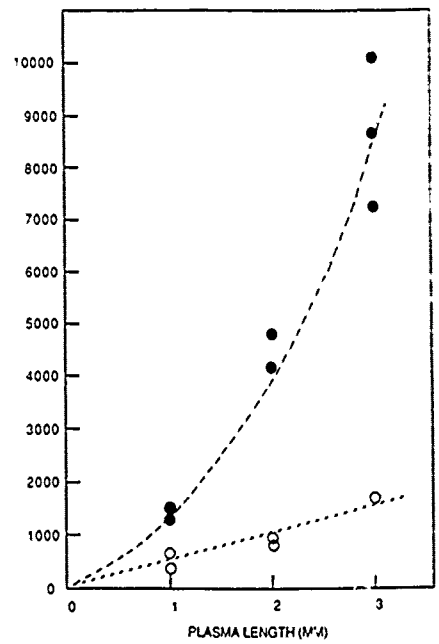

Fig. 3. Intensities of C VI 18.22 nm (filled circles) and 13.50 nm (open circles) versus plasma length with 25 J of laser energy and a magnetic-field strength of 50 kG. A stainless-steel blade was placed in front of the target for rapid cooling. The dashed curve is a theoretical gain curve of 8.1 cm^{-1}; C VI 13.50 nm increases linearly.

$$I \sim \frac{(e^G - 1)^{3/2}}{(Ge^G)^{1/2}}, \quad (1)$$

which describes the output intensity of a Doppler-broadened, homogeneous source of amplified spontaneous emission of gain–length product G. The theoretical gain curve of $g = 8.1\ \mathrm{cm}^{-1}$ is shown in Fig. 3. It can clearly be seen that the C VI 18.22-nm line increases exponentially and that the C VI 13.50-nm line increases linearly with the plasma length. The 13.50-nm line is expected to have much less gain than the 18.22-nm line owing to its lower transition rate and shorter wavelength.

In conclusion, we have demonstrated a high gain of $8 \pm 2\ \mathrm{cm}^{-1}$ at 18.22 nm in C VI using the newly developed carbon target system pumped with a 25-J, 3-nsec Nd:glass laser. We plan to combine this amplifier with the present soft-x-ray 18.22-nm laser in a CO_2-laser-produced, magnetically confined carbon plasma in order to increase the beam energy. The output energy is an important issue for the application of a soft-x-ray laser to x-ray microscopy and may be a significant obstacle in the utilization of systems with a small aperture of the lasing medium.[13]

We thank H. Furth and W. Tighe for helpful discussions and D. Voorhees, G. Drozd, D. Dicicco, and B. Micholvic for their technical support in making the new system and providing length-varying cylindrical targets. G. Umesh thanks the government of India for supporting him with a postdoctoral fellowship. This research was supported by the U.S. Department of Energy, Advanced Energy Projects of Basic Energy Sciences, and the U.S. Air Force Office of Scientific Research.

G. Umesh is a visiting physicist from the Indian Institute of Technology, New Delhi, India.

S. Suckewer is also with the Department of Mechanical and Aerospace Engineering, Princeton University.

References

1. D. Matthews, M. Rosen, S. Brown, N. Ceglio, D. Eder, A. Hawryluk, C. Keane, R. London, B. MacGowan, S. Maxon, D. Nilson, J. Scofield, and J. Trebes, J. Opt. Soc. Am. B 4, 575 (1987).
2. M. Howells, C. Jacobsen, J. Kirz, R. Feder, K. McQuaid, and S. Rothman, Science 238, 514 (1987).
3. H. C. Kapteyn, R. W. Lee, and R. W. Falcone, Phys. Rev. Lett. 57, 2939 (1986).
4. M. H. Sher, J. J. Macklin, J. F. Young, and S. E. Harris, Opt. Lett. 12, 891 (1987).
5. C. H. Skinner, D. Kim, A. Wouters, D. Voorhees, and S. Suckewer, in *X-Ray Microscopy II*, D. Sayre, M. Howells, J. Kirz, and H. Rarback, eds. (Springer-Verlag, Berlin, 1988), p. 36.
6. S. Suckewer, C. H. Skinner, D. Kim, E. Valeo, D. Voorhees, and A. Wouters, Phys. Rev. Lett. 57, 1004 (1986).
7. D. Kim, C. H. Skinner, A. Wouters, E. Valeo, D. Voorhees, and S. Suckewer, J. Opt. Soc. Am. B 6, 115 (1989).
8. C. W. Clark, M. G. Littman, R. Miles, T. J. McIlrath, C. H. Skinner, S. Suckewer, and E. Valeo, J. Opt. Soc. Am. B 3, 371 (1986); S. Suckewer, C. H. Skinner, D. Kim, E. Valeo, D. Voorhees, and A. Wouters, J. Phys. (Paris) 47C3, 23 (1986).
9. P. Jaeglé, G. Jamelot, A. Carillon, A. Klisnick, A. Sureau, and H. Guennou, J. Opt. Soc. Am. B 4, 563 (1987), and references therein.
10. V. A. Bhagavatula and B. Yaakobi, Opt. Commun. 24, 331 (1978).
11. R. L. Kelly and L. J. Palumbo, in *Atomic and Ionic Emission Lines Below 2000 Angstroms; Hydrogen through Krypton*, NRL Rep. 7599 (Naval Research Laboratories, Washington, D.C., 1973).
12. G. J. Linford, E. R. Peressini, W. R. Sooy, and M. L. Spaeth, Appl. Opt. 13, 379 (1974).
13. C. Chenais-Popovics, R. Corbett, C. J. Hooker, M. H. Key, G. P. Kiehn, L. S. Lewis, G. J. Pert, C. Regan, S. J. Rose, S. Sadaat, R. Smith, T. Tomie, and O. Willi, Phys. Rev. Lett. 59, 2161 (1987).

Reprint Series
30 March 1990, Volume 247, pp. 1553–1557

SCIENCE

Soft X-ray Lasers and Their Applications

S. SUCKEWER AND C. H. SKINNER

Soft X-ray Lasers and Their Applications

S. SUCKEWER AND C. H. SKINNER

The emerging technology of soft x-ray lasers has novel applications to microscopy, lithography, and other fields. This article describes the status of soft x-ray laser research with the aim of bringing the rapid developments in this field to the attention of potential users in other disciplines. The different techniques for generating a population inversion and producing a soft x-ray laser are reviewed. The status of current research in the field and the near-term prospects are described. It is expected that the range of potential applications of soft x-ray lasers will increase as their performance improves. Work aimed at increasing the output power and progressing to shorter wavelengths with these devices is also reviewed.

LASERS OPERATING AT X-RAY WAVELENGTHS HAVE BEEN sought after since the invention of the first lasers in 1960, because of their intrinsic interest and also because their ultrahigh brightness and short wavelengths made them ideal for a variety of applications. However, the creation of a population inversion in highly ionized ions necessary for x-ray laser action places severe demands on the required pump source, and for this reason soft x-ray lasers remained an elusive dream until 1984. The first demonstration of lasing action in the soft x-ray region by groups at Lawrence Livermore National Laboratory and Princeton University in 1984 has been followed by work at a number of laboratories around the world. At present, rapid progress is being made in the extension of the operating wavelength range and power of these devices and in the development of small-scale and relatively low-cost soft x-ray lasers suitable for widespread application to fields such as microscopy and microelectronics.

Recent work at a number of laboratories has been aimed toward the development of soft x-ray lasers in wavelength regions shorter than 20 nm and of lasers in the vacuum-ultraviolet (VUV) region near 100 nm and below. Noteworthy are the achievements of very high gain (much above saturation) in Cs near 90 nm with relatively low pumping power as demonstrated by the Stanford group (*1*), the generation of very high power density radiation (above 10^{18} W cm^{-2}) for application to soft x-ray lasers by the Chicago group (*2*), and theoretical work on "tabletop" VUV lasers at 30 to 40 nm with the use of Ni-like or Nd-like ions by the Massachusetts Institute of Technology group (*3*). The experimental and theoretical work at Princeton (*4–8*) includes: (i) the development of a powerful subpicosecond laser system that uses a new approach in x-ray laser development to generate soft x-ray spectra, (ii) a theoretical model for atoms in very strong electromagnetic fields; and (iii) improvement of the present 18.2-nm laser and its application to soft x-ray microscopy. The existing soft x-ray laser at Princeton is pumped by a commercial 300-J CO_2 laser and has a wavelength of 18.2 nm, an output energy of 1 to 3 mJ, a pulse duration of 10 to 30 ns, and a beam divergence of 5 mrad.

The authors are at the Princeton University Plasma Physics Laboratory, Princeton, NJ 08543. S. Suckewer is also affiliated with the Mechanical and Aerospace Engineering Department of Princeton University.

Soft X-ray Laser Research

Although soft x-ray laser research was pursued in the 1970s, the field came of age in 1984 with the first unambiguous demonstration of high gain by groups at Lawrence Livermore National Laboratory (*9*) and Princeton University (*10*). These two groups used different approaches to generate gain (see Fig. 1), and these approaches have formed the basis of all successful work on soft x-ray lasers since that time. (i) The recombination approach is based on H-like or Li-like ions. (ii) The collisional excitation approach is based on Ne-like or Ni-like ions.

Both schemes rely on high-power pulsed lasers to create the appropriate conditions in a plasma, and in both schemes the population inversion necessary for stimulated emission and gain is brought about by fast radiative decay of the lower level. In the recombination approach for H-like ions, a laser is used to create a plasma with a high fraction of totally stripped ions. After the laser pulse, the plasma is cooled rapidly and undergoes fast three-body recombination. In some cases the plasma is cooled by adiabatic expansion. One unique feature of the Princeton laser is that the plasma is confined in a magnetic field and cooled by radiation losses The magnetic field maintains a high electron density, which is beneficial because the three-body recombination rate scales as the electron density squared. It also helps to shape the plasma into a long thin geometry suitable for a laser and enables an efficiency to be attained that is almost 100 times higher than other operational soft x-ray laser systems. Three-body recombination puts into upper excited levels a high population, which decays downward by collisional radiative cascade. In hydrogenic ions, level 2 decays rapidly by radiation and a population inversion is built up between levels 3 and 2. The atomic structure of Li-like ions is similar to that of H-like ions, and the same approach works in this system also (*11, 12*). In this case the 3–2 transitions have a high radiative decay rate, and gain can be generated on the 4–3 and 5–3 transitions The Li-like sequence has the advantage of a shorter wavelength lasing transition for ions of similar ionization potential, that is, a better "quantum efficiency."

The Ne-like scheme was applied at Lawrence Livermore National Laboratory. Here a high-density, high-temperature plasma is generated by a large Nd laser, Novette or Nova. In the Ne-like plasma, a large population of ions is collisionally excited to the $3p$ level. The $3s$ level has a relatively low population since it has a fast radiative transition to ground, and a population inversion is built up between

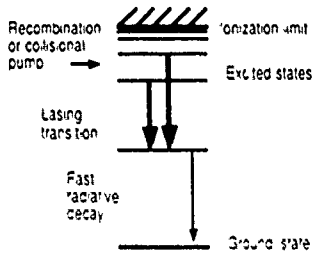

Fig. 1. Partial energy level diagram of the two successful soft x-ray laser schemes.

the $3p$ and $3s$ levels. The same scheme also works in Ni-like ions, and here, as in the case of Li-like ions, there is an advantage in using the Ni-like sequence to access the shortest possible wavelengths. A recent review of work at Livermore is given in (*13*). The ambitious goal of the Livermore work is to develop a high-brightness, high-coherence soft x-ray laser in the wavelength range 4.0 to 5.0 nm for high-resolution holographic imaging of biological specimens. One step in this direction was the recent achievement of a gain-length (GL) of ≈4 at 4.48 nm in Ni-like Ta. In summary, both approaches use a laser to create an appropriate plasma and rely on fast radiative decay to deplete the lower level in order to generate a population inversion. The major difference is that in one case the upper level is populated through recombination and in the other it is populated by collisional excitation.

A number of laboratories around the world are heavily engaged in soft x-ray laser research. We would like to mention the pioneering work of Pert and Ramsden and their colleagues (*14*) at Hull in England on the recombination scheme for C fibers at 18.2 nm, which was later taken up at the Rutherford Appleton Laboratory (*15*). This work is now part of an international effort involving seven different institutions in England, France (Orsay), Japan (Institute for Laser Engineering), and the United States (Naval Research Laboratory). The soft x-ray laser experiments of Jaeglé *et al.* (*11*) originated from the observation of a bright line at 10.57 nm in an Al plasma. This previously unknown line was identified as the $3d$–$5f$ line of Li-like Al. Confirmation that this line was due to amplification of spontaneous emission was obtained from measurements of the plasma absorption or gain over the observed spectrum. A clear peak was seen at 10.57 nm, corresponding to a gain of up to 2.5 cm^{-1}. More recently, experiments with a 6-cm-long plasma have resulted in a gain-length of $GL \approx 3.0$. Use of a soft x-ray mirror with a reflectivity of 5% in a double-pass arrangement resulted in an effective gain-length of $GL \approx 4$. Gain-lengths of up to $GL \approx 2.7$ on the $3d$–$4f$ and $3d$–$5f$ transitions in Li-like Al have also been reported by Moreno *et al.* (*16*).

The recombination approach has been used at the Laboratory for Laser Energetics at Rochester University (*17*) to produce gain on the C VI 18.2-nm transition in a radiation-cooled Se/Formvar plasma. The collisional excitation scheme has also been demonstrated by a group at the Naval Research Laboratory (*18*) at wavelengths from 19.5 to 28.5 nm in Ne-like Ge and Cu. This experiment used less demanding technology than the scheme at Livermore: a lower power driver laser (350 to 485 J operating at the fundamental wavelength of 1.05 μm) and simple slab targets rather than exploding foils. Interestingly, the $J=2$–$J=1$ gain coefficient (J is the angular momentum quantum number) of $G \approx 4$–1 cm^{-1} observed with single-sided illumination of a thick slab of Ge was comparable to that obtained by the Livermore group with an Se film target that was illuminated from both sides. Also for the first time the Cu $J=0$ to $J=1$ line showed a G comparable to that for the $J=2$–$J=1$ lines, in agreement with theoretical predictions. In Japan, Herman *et al.* (*19*) have demonstrated gain at various wavelengths including a measurement of G of 2 cm^{-1} in the 8.1-nm transition in H-like F. Kato *et al.* (*20*) have reported $GL = 1$ at 5.4 nm and $GL = 0.9$ at 4.5 nm, but their experimental data have been criticized as being ambiguous and unconvincing. Very recently there has been a report by Hara *et al.* (*21*) of gain in the soft x-ray region produced by a small-scale (6-J) pump laser. The presence of gain was deduced from the nonlinear rise in intensity with length of Al X and Al XI emission lines. However, in contrast to earlier work by Kim *et al.* (*5, 6, 12*), the nonlinear rise of the "gain lines" with plasma length was not referenced to a linear rise of "no-gain lines" in Al XI such as the 14.1-nm transition, leaving open the possible influence of other effects (such as gradients in the plasma temperature along the plasma region viewed by the detector) that could also produce a nonlinear intensity rise. Clarification of this point would be valuable as this result, if verified, would add to earlier work (*5, 6*) with very favorable implications for the commercialization of soft x-ray lasers.

A third potential method to achieve soft x-ray lasing is resonant

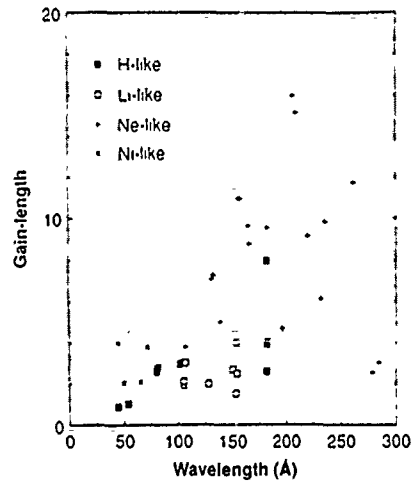

Fig. 2. Plot of gain-length achieved to date versus wavelength (*5–20*). The dashed line marks $GL = 4.6$, which corresponds to an enhancement of 10.

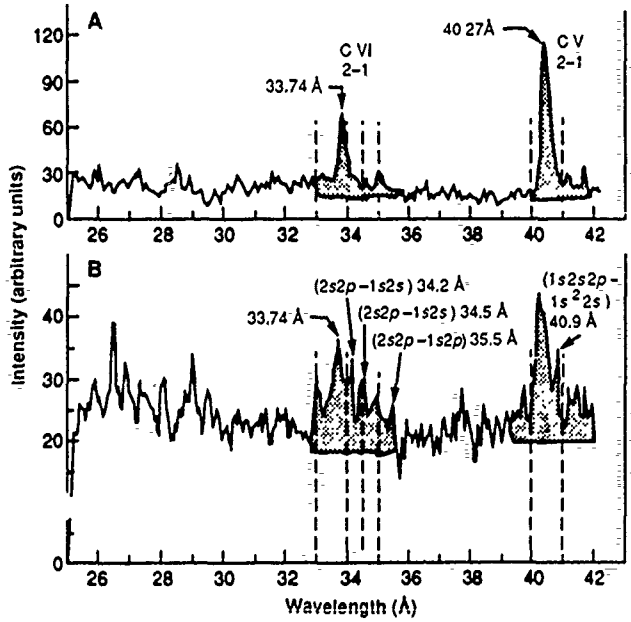

Fig. 3. Carbon spectra obtained with a Teflon target (**A**) without pulse compression [20-GW laser power; $E = 20$ mJ (200 shots), $\Delta t = 1$ ps] and (**B**) with pulse compression and final KrF* amplifier [0.3-TW laser power, $E = 100$ mJ (5 shots), $\Delta t = 300$ fs]. [Adapted from (*4*) with permission of the Optical Society of America]

photopumping in a two-component plasma (22). Resonant photoexcitation has been recently demonstrated in the soft x-ray range by Monier *et al.* (23). A H-like Al XIII resonance line was used to pump a Ne-like Sr XXIX resonance line, resulting in an increase of a factor of 2 in fluorescence from the upper state of the pumped transition. However, the pumping efficiency was less than expected. Several difficulties need to be overcome if this method is to be successfully applied to generating soft x-ray lasing.

The current state of the art is represented in Fig. 2, which shows *GL* versus wavelength. High *GL* values have been achieved over a variety of wavelengths, although in general there is a falloff in gain as the wavelength approaches the "water window" region, 2.4 to 4.4 nm, important for biological applications. It is only when *GL* exceeds 4.6 that the output intensity exceeds spontaneous emission by more than an order of magnitude and one can talk about a soft x-ray laser beam. A number of groups are investigating the physics relevant to more efficient or shorter wavelength schemes, in particular Harris and his colleagues (24) and Murnane *et al.* (25), who are working on Auger ionization, and Boyer *et al.* (26), who are working on multiphoton processes. More details of the current research directions are contained in (27). For special journal issues devoted to soft x-ray lasers, see (28, 29).

Soft X-ray Laser Research at Princeton

Approach toward a 1-nm x-ray laser. The main difficulty in approaching shorter and shorter wavelengths is the requirement for very large increases in pumping power. For example, for soft x-ray lasers pumped primarily by recombination or electron-excitation processes, the pumping power P is proportional approximately to λ^{-4} for constant gain G. This follows from a simple relation between gain, wavelength λ, and population inversion ΔN_{inv} [see (30)].

$$G \sim \lambda^3 \Delta N_{inv}$$

where

$$\Delta N_{inv} \sim P$$

Therefore, in order to decrease the lasing wavelength from 10 to 1 nm, the pumping power must be increased approximately by a factor of 10^4.

The recombination laser at Princeton presently operating at 18.2 nm requires a laser pumping energy of ~300 J. Without changing pulse length, the energy for lasing at 1 nm would need to be on the order of tens of megajoules. Because the size and cost of a laser increase dramatically with energy (but not with power), such a system would be very large and very expensive. Thus, a great deal of attention in soft x-ray laser development is being devoted to schemes in which metastable and autoionizing levels can be used for storing pumped energy, as proposed by Harris (31), or schemes based on very short (picosecond and subpicosecond) pumping pulses (32). This second approach is particularly attractive because the upper state lifetime is of the order of 10^{-12} to 10^{-13} s for a transition wavelength of ≈1 nm. Therefore, pumping is required only for a picosecond or subpicosecond time interval. After this time, energy would just be wasted in heating the target material.

Lasers with beam energy of order of only 1 J and pulse duration of 1 ps can provide very high power, $P \sim 10^{12}$ W. Even more important, such a laser operating in the UV range (for example, the KrF excimer laser with wavelength 0.25 μm) can be focused to a 2- to 3-μm spot, providing a power density in excess of 10^{18} W cm^{-2} (with corresponding electric field $\sim 10^{11}$ V cm^{-1} = 10 kV nm^{-1}) on target. With this power density it is possible to provide multiphoton excitation and multiphoton ionization of highly ionized ions and use such processes for the creation of population inversion and gain at wavelengths down to 1 nm.

It is very difficult, however, to both create highly ionized ions and provide selective multiphoton excitation of such ions with a single laser. Therefore, we proposed in 1986 the use of two lasers (33). The role of the first, high energy but low-power laser (for example, 0.5-kJ, 50-ns CO_2 or 100-J, 3-ns Nd/YLF laser, where YLF is yttrium lanthanum fluoride) is to create a plasma column of highly ionized ions that may be confined in a strong magnetic field. The role of the second, extremely high power laser (~1-TW KrF laser) is to generate gain by multiphoton ionization, very fast ionization (for example, inner shell ionization), or selective multiphoton excitation. More details about the Powerful Picosecond (Sub-Picosecond) Laser (PP-Laser) system are presented by Meixler *et al.* (4).

One of our first experiments with such a high-power density laser beam was a measurement of soft x-ray spectra for C and F. The laser beam was focused on a rotating cylindrical Teflon target while a soft x-ray, grazing incidence Schwob-Fraenkel spectrometer (SOXMOS) with multichannel detector monitored the plasma radiation from the target surface. Figure 3B shows the spectrum in the vicinity of the C VI 3.37-nm and C V 4.03-nm lines (both from $2 \rightarrow 1$ transitions). In addition to the enormous line broadening, one can see a strongly pronounced, unusual structure in the lines. Both broadening and satellite structure are larger in the spectrum obtained at high power than in the spectrum obtained at lower power (Fig. 3A). On the red side of the lines, several satellite lines can be identified ($2p2s$–$1s2s$ at 3.42 and 3.45 nm, $2s^2$–$1s2p$ at 3.55 nm, and $1s2s2p$–$1s^22s$ at 4.09 nm). In addition, there is a component at 3.3 nm on the blue side of the C VI 3.37-nm line. It should also be noticed that the number of shots needed for these short-wavelength spectra is proportional not to the laser beam energy but rather to its power. (The energy of the laser beam increased by a factor of 5 while the number of shots decreased by a factor of 20.) In spectra obtained earlier with the 20- to 30-GW PP-Laser (10^{16} W cm^{-2}), part of the large broadening and asymmetry of the F VII lines in the spectral region from 12.0 to 14.0 nm was attributed to the Stark effect and radiation from the forbidden components of the lines (34). Very recently, Koshelev (35) interpreted asymmetric broadening of the F VII lines to be a result of satellite line radiation. Spectral lines of C VI, C V, and F VII excited by the very high power beam seem to indicate a complicated satellite-type structure. Of course, the very strong electric field created by such a laser beam may be partially responsible for these effects. Spectroscopic measurements for different targets as well as experiments in which a highly ionized plasma is initially generated by CO_2 or Nd/YLF lasers and then excited by the PP-Laser should enable us to develop a clearer picture of the behavior of highly ionized ions in strong laser fields.

Development of an additional amplifier at 18.2 nm. Presently, the highest beam energy of our soft x-ray laser (SXL) (36) at 18.2 nm (C VI 3–2 transition) pumped by a 300-J CO_2 laser in a 90-kG solenoidal magnetic field is 3 mJ with a 3-min repetition rate. At present, the beam energy is one of the most important parameters for applications of the SXL. In order to increase it, we have developed an additional SXL amplifier (3 mm long) at 18.2 nm that is pumped by a Nd/YLF laser beam line-focused onto a C target. Thin Fe blades in the front of the targets provide additional radiation cooling of the plasma column. We have demonstrated gain up to $G \approx 8$ cm^{-1} in one SXL amplifier with 15 J of Nd/YLF laser beam energy on target [see Kim *et al.* (5, 6)]. The axial spectra in the vicinity of the lasing line C VI 18.2 nm (3–2 transition) and in the vicinity of C VI 13.5 nm (4–2 transition) were measured for 1-, 2-, and 3-mm-long targets. A striking, nonlinear increase in the intensity of the 18.2-nm line, in comparison to near-linear increase in intensity of the 13.5-nm line, may be seen in Fig. 4.

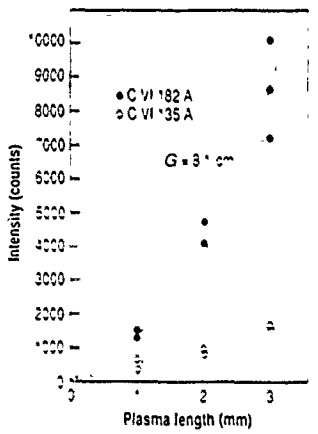

Fig. 4. Gain measurement for C VI 18.2 nm with the use of 15-J pump laser energy on target (25 J in total beam; 50 kG, stainless steel blade). [Adapted from (*6*) with permission of the Optical Society of America]

Cavity development. A laser cavity can increase the brightness of the SXL beam by several orders of magnitude by decreasing the divergence to a value close to the diffraction limit. In order to establish the proper cavity modes, a number of passes through the gain medium are needed and a relatively long-duration gain is necessary ($GL > 4$ for several cavity round-trip times). In our early work, using a newly developed multilayer mirror (*37*), we demonstrated a 120% increase in 18.2-nm radiation, due to amplification of stimulated emission, by using a mirror with a reflectivity of only 12% (*38*). However, the mirror alignment posed tremendous difficulties, which practically made it impossible to develop a cavity in the original SXL setup. We have therefore designed an unstable resonator-type cavity with a transversely pumped C fiber as the lasing medium. The same cavity will also be used for a 1-cm-long SXL created by a line-focused Nd/YLF laser beam incident on the cylindrical C target described in the section on an additional amplifier.

In the cavity design, particularly in choosing distances between lasing medium and mirrors, we were concerned with the possibilities of damaging the multilayer mirrors by soft x-ray radiation. Recently, however, Ceglio *et al.* (*39*) demonstrated, in a very elegant cavity experiment, that such mirrors are quite stable against soft x-ray beam damage, even at a distance of a few centimeters from the lasing medium.

Gain in Li-like ions at 15.4 and 12.9 nm. Pioneering work for Li-like Al XI ions, particularly for the $5f$–$3d$ transition at 10.5 nm, was done by Jaegle and his group (*11*), using a Nd/glass laser (initial plasma electron density $N_e = 10^{21}$ cm^{-3}) for the pumping lasing medium. In our system with a CO_2 pump laser the initial electron density is $N_e = 10^{19}$ cm^{-3}. For such an electron density, the largest gain in Al XI and Si XII is expected for the $4f$–$3d$ transitions at 15.4 nm and 12.9 nm, respectively. The Al or Si targets used in the experiment were very similar to the SXL C target with the exception that the blades were a combination of lasing element (Al or Si) and fast radiator (Fe). The measured one-pass gain was $GL \approx 3$ to 4 for 15.4-nm radiation and $GL \approx 1$ to 2 for 12.9-nm radiation. Details about the experiment and theoretical modeling are presented in (*5*, *12*).

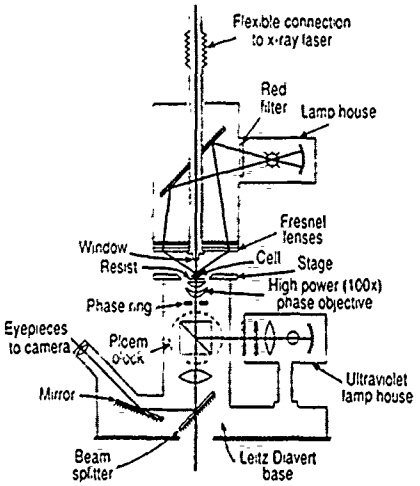

Fig. 5. *Schematic of* the COXRALM designed to allow biologists to select and observe live cells before recording a high-resolution contact image with the soft x-ray laser.

Application of the Soft X-ray Laser to Microscopy

Most of what is known about the internal structure of cells has been learned by the development and application of the techniques of electron microscopy. This knowledge rests on the premise that the intensive procedures necessary to prepare a specimen for electron microscopy do not significantly influence the structure, form, and high-resolution detail observed. Nonetheless, unanswered questions remain about the fidelity of the image of a cell that has been fixed, stained with heavy metals, and sectioned to the original living cell. X-ray microscopy offers a new way to look at unaltered cells in their natural state. The absorption edges in the x-ray spectra of naturally occurring cell constituents provide contrast without the addition of heavy metals to the cell necessary in electron microscopy. Work has begun in using high-brightness synchrotrons and soft x-ray lasers as light sources for x-ray microscopy (*40*). Biologists have long dreamed of observing the form and function of living cells at high resolution. The short, nanosecond pulse length of soft x-ray lasers offers the potential of observing a cell that was alive the instant before a flash exposure of a soft x-ray laser recorded its image. The necessary radiation dose levels make it unlikely that the cell will survive the exposure, but exposures of different cells should make it possible to piece together new information about dynamic processes inside cells.

Work has begun at Princeton to use the 18.2-nm laser (SXL) for soft x-ray contact microscopy of biological specimens. (This work is also closely related to x-ray microlithography.) The ultimate goal of our x-ray laser microscopy program is to obtain images of living cells. The details of this work as well as our other work with soft x-ray laser microscopy are described in (*7*, *41*, *42*).

In the x-ray laser microscope, a thin (~0.1-μm) silicon nitride window square separates the vacuum tube, in which x-rays travel, from the biological cells located on photoresist at atmospheric pressure. We have demonstrated that the SXL beam has sufficient energy to expose images on photoresist in a single shot. In x-ray contact microscopy, magnification is obtained when the exposed photoresist is viewed in a scanning electron microscope (SEM). Images of diatom fragments (the silicified skeleton of planktonic algae) on photoresist indicated that the resolution on the photoresist was better than 0.1 μm. One may also regard diatom fragments as a kind of lithographic mask and an illustration of the potential application of the SXL to microlithography.

We have built a Composite Optical/X-ray Laser Microscope (COXRALM), shown schematically in Fig. 5 and described in (*7*, *42*). COXRALM is designed to allow a biologist to select and observe live biological cells, using an optical phase-contrast microscope (*43*), and then create a high-resolution image of the cells on photoresist with the SXL beam. The first results were obtained with dehydrated cells to optimize image contrast and resolution without the technicalities of handling wet, live cells. Figure 6 shows a SEM image of a replica produced by the 18.2-nm SXL of dehydrated

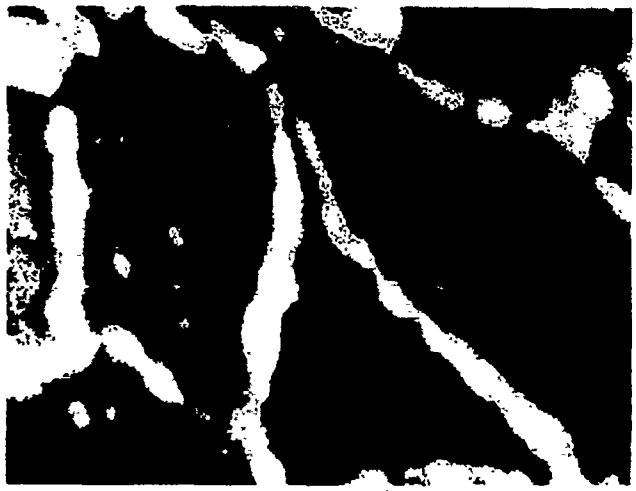

Fig. 6. False-color SEM image of a replica of a HeLa cell that was subject to a viral infection. The replica was generated by contact microscopy with the 18.2-nm laser. The computer-generated false color enhances the contrast of the cell features. Scale bar, 10 μm.

HeLa cells (Helen Lane cervical cancer cells) obtained from the Biology Department of Princeton University. Presently our work is concentrated on experiments with live cells in a wet environment and on the development of a new Imaging Soft X-ray Laser Microscope (IXRALM).

Future Prospects

Rapid progress in soft x-ray laser development has been made. Especially exciting is progress in the miniaturization of soft x-ray lasers and the start of work on their applications. The general impact soft x-ray lasers will have in science and technology will depend on improvements in both their performance and their cost. It is necessary for their successful commercialization that these devices operate routinely at high gain-lengths ($GL > 4$), with the use of a low-cost driver laser, and this needs more system development and engineering. Most applications of visible-wavelength lasers are based on the fact that the brightness of these lasers is several orders of magnitude greater than that of conventional spontaneous emission sources, and this is achieved principally by the laser cavity mirrors. This technology is significantly more difficult in the x-ray region because of intrinsic limitations of x-ray absorption in materials and present limits in the soft x-ray laser pulse lengths. Nonetheless, a "revolution" (*44*) in x-ray optics is under way and the precedent of visible-wavelength lasers illustrates the potential benefits awaiting the creative inventor of applications of this technology to novel fields.

REFERENCES AND NOTES

1. C. P. Barty *et al.*, *Phys. Rev. Lett.* **61**, 2201 (1988).
2. K. Boyer *et al.*, in *Short Wavelength Coherent Radiation: Generation and Applications*, R. W. Falcone and J. Kirz, Eds. (Optical Society of America, Washington, DC, 1989), vol. 2, p. 220.
3. P. L. Hagelstein, *ibid.*, p. 28.
4. L. Meixler *et al.*, *ibid.*, p. 106.
5. D. Kim *et al.*, *ibid.*, p. 116; S. Suckewer, *ibid.*, p. 36
6. D. Kim, C. H. Skinner, G. Umesh, S. Suckewer, *Opt. Lett.* **14**, 665 (1989).
7. D. S. DiCicco *et al.*, in *Short Wavelength Coherent Radiation: Generation and Applications*, R. W. Falcone and J. Kirz, Eds. (Optical Society of America, Washington, DC, 1989), vol. 2, p. 277.
8. S. M. Susskind, S. C. Cowley, E. J. Valeo, *ibid.*, p. 251
9. D. L. Matthews *et al.*, *Phys. Rev. Lett.* **54**, 110 (1985).
10. S. Suckewer, C. H. Skinner, H. Milchberg, C. Keane, D. Voorhees, *ibid.* **55**, 1753 (1985).
11. P. Jaeglé *et al.*, *Europhys. Lett.* **7**, 337 (1988); P. Jaeglé *et al.*, *J. Opt. Soc. Am. B* **4**, 563 (1987).
12. D. Kim *et al.*, *J. Opt. Soc. Am. B* **6**, 115 (1989).
13. C. J. Keane *et al.*, *J. Phys. B* **22**, 3343 (1989).
14. D. Jacoby, G. J. Pert, S. A. Ramsden, L. D. Shorrock, G. J. Tallents, *Opt. Commun.* **37**, 193 (1981).
15. C. S. Lewis *et al.*, *Plasma Phys. Controlled Fusion* **30**, 35 (1988).
16. C. Moreno, H. R. Griem, S. Goldsmith, J. Knauer, *Phys. Rev. A* **39**, 6033 (1989).
17. J. F. Seely *et al.*, *Opt. Commun.* **54**, 289 (1985).
18. T. N. Lee, E. A. Maclean, R. C. Elton, *Phys. Rev. Lett.* **59**, 1185 (1987).
19. P. R. Herman, T. Tachi, K. Shihoyama, H. Shiraga, Y. Kato, *IEEE Trans. Plasma Sci.* **16**, 520 (1988).
20. Y. Kato *et al.*, in *Short Wavelength Coherent Radiation: Generation and Applications*, R. W. Falcone and J. Kirz, Eds. (Optical Society of America, Washington, DC, 1989), vol. 2, p. 47
21. T. Hara, K. Ando, N. Kusakabe, H. Yashiro, Y. Aoyagi, *Jpn. J. Appl. Phys.* **28**, 1010 (1989).
22. A. V. Vinogradov, I. I. Sobelman, E. A. Yukov, *Kvantovaya Elektron. (Moscow)* **2**, 105 (1975) [*Sov. J. Quant. Electron.* **5**, 59 (1975)].
23. P. Monier, C. Chenais-Popovics, J. P. Geindre, J. C. Gauthier, *Phys. Rev. A* **38**, 2508 (1988).
24. S. E. Harris and J. F. Young, *J. Opt. Soc. Am. B* **4**, 547 (1987); M. H. Sher, J. J. Macklin, J. F. Young, S. E. Harris, *Opt. Lett.* **12**, 891 (1987).
25. M. M. Murnane, H. C. Kapteyn, R. W. Falcone, in *Short Wavelength Coherent Radiation: Generation and Applications*, R. W. Falcone and J. Kirz, Eds. (Optical Society of America, Washington, DC, 1989), vol. 2, p. 189.
26. K. Boyer *et al.*, *ibid.*, p. 220.
27. R. W. Falcone and J. Kirz, Eds., *Short Wavelength Coherent Radiation: Generation and Applications* (Optical Society of America, Washington, DC, 1989), vol. 2.
28. Special issue on "Atomic and plasma processes in x-ray lasers," *IEEE Trans. Plasma Sci.* **16**, 469–563 (1988).
29. Special issue on "The generation of coherent XUV and soft x-ray radiation," *J. Opt. Soc. Am. B* **4**, 530–609 (1987).
30. R. W. Waynant and R. C. Elton, *Proc. IEEE* **64**, 1059 (1976).
31. S. E. Harris, *Opt. Lett.* **5**, 1 (1980).
32. T. S. Luk *et al.*, *Phys. Rev. Lett.* **51**, 110 (1983).
33. C. W. Clark *et al.*, *J. Opt. Soc. Am. B* **3**, 371 (1986).
34. C. H. Nam *et al.*, *Phys. Rev. Lett.* **59**, 2427 (1987).
35. K. N. Koshelev, *J. Phys. B* **21**, L593 (1988).
36. S. Suckewer *et al.*, *Phys. Rev. Lett.* **57**, 1004 (1986).
37. T. W. Barbee, Jr., S. Mrowka, M. C. Hettrick, *Appl. Opt.* **24**, 883 (1985).
38. C. Keane *et al.*, *Rev. Sci. Instrum.* **57**, 1296 (1986).
39. N. Ceglio *et al.*, *Opt. Lett.* **13**, 108 (1988).
40. D. Attwood and B. Barton, Eds., *X-ray Microimaging for the Life Sciences: Proceedings of the Workshop [Lawrence Berkeley Lab. Rep. LBL-27660* (August 1989)].
41. C. H. Skinner *et al.*, *IEEE Trans. Plasma Sci.* **16**, 512 (1988).
42. C. H. Skinner *et al.*, *J. Microsc.*, in press.
43. J. Hirschberg *et al.*, *Am. Chem. Soc. Symp. Ser. 102* (1979), p. 262
44. N. M. Ceglio, *J. X-ray Sci. Technol.* **1**, 7 (1989).

45. The data presented here were the results of dedicated work by members of the scientific and technical staff and graduate students of the Princeton University X-ray Laser Project: D. S. DiCicco, D. Kim, K. Krushelnik, L. D. Meixler, C. H. Nam, J. Robinson, R. J. Rosser, S. Susskind, W. Tighe, E. J. Valeo, D. Voorhees, and A. Wouters, by visiting scientists, particularly J. L. Schwob and G. Umesh, and by a number of scientists associated with us, among them, I. Bernstein, C. Clark, P. C. Cheng, S. C. Cowley, V. Feldman, J. Fujimoto, J. Goldhar, A. Gupta, J. Hirschberg, E. Kohen, R. Kulsrud, M. Littman, T. Mellilrath, R. Miles, C. Oberman, and J. Seely. We thank H. Furth for helpful discussions, stimulation of the work on applications of the SXL, and continuing support and encouragement. The work was supported by the U.S. Department of Energy Advanced Energy Projects of Basic Energy Sciences (grant KC-05-01) and the U.S. Air Force Office of Scientific Research (contract AFOSR-86-0066).

Reprinted from Journal of the Optical Society of America B, Vol. 6, page 115, January 1989

Soft-x-ray amplification in lithiumlike Al XI (154 Å) and Si XII (129 Å)

D. Kim, C. H. Skinner, A. Wouters, E. Valeo, D. Voorhees, and S. Suckewer

Plasma Physics Laboratory, Princeton University, Princeton, New Jersey 08543

Received January 7, 1988; accepted September 19, 1988

Recent experiments on soft-x-ray amplification in lithiumlike ions in a CO_2 laser produced recombining plasma confined in a magnetic field are presented. The maximum gain-length (GL) products observed are GL $\simeq$ 3–4 for the 154-Å $4f$–$3d$ transition in Al XI and GL $\simeq$ 1–2 for the 129-Å $4f$–$3d$ transition in Si XII. A one-dimensional hydrodynamic code with a collisional-radiative atomic model was used to model the plasma, and the theoretical predictions of gain agree well with the observations. Descriptions of both hydrodynamic and atomic physics codes are given.

1. INTRODUCTION

Since the demonstration of high amplification of soft x rays in laser-produced plasmas,[1,2] different approaches to improve x-ray laser characteristics to shorter wavelengths, higher power, better coherence, narrower divergence, and better efficiency are being pursued at several laboratories.[3–11] In terms of improving the power, coherence, and divergence, we have developed an experimental system with which a series of experiments on soft-x-ray laser cavities will be performed. An x-ray laser operating wavelength between the K edge of carbon at 44 Å and that of oxygen at 25 Å would be optimal in terms of penetration, contrast, and resolution for microscopy of biological specimens.

At Princeton University we are using two approaches to make a shorter-wavelength, soft-x-ray laser. One approach is to produce a population inversion in Kr- or Ar-like ions through selective excitation by multiphoton transitions[12] or inner-shell ionizations. The inner-shell ionization scheme was proposed initially by Duguay and Rentzepis,[13] modified later by McGuire,[14] and recently demonstrated experimentally at 1089 Å.[8,9] In our approach the plasma of the desired ionization stage will be produced by a CO_2 or Nd:glass laser and then, through multiphoton transitions or inner-shell ionizations, will be excited by a powerful picosecond laser. The instrumentation for this approach has been developed, and a series of experiments is planned for the near future.

The subject of this paper is an approach based on a recombination scheme using magnetically confined (≤100-kG) Li-like ions produced by an ~500-J, 50–70-nsec CO_2 laser. This scheme has been successfully used to make a soft-x-ray laser in H-like C VI with the following characteristics: 182-Å wavelength, amplification by a factor of 500, 1–3-mJ pulse energy, 10–30-nsec pulse duration, and 5-mrad beam divergence.[6]

An extensive series of experiments for developing a soft-x-ray laser using Li-like ions has been performed by Jaeglé *et al.*[5] In these experiments a Nd laser produces a freely expanding plasma, generating a population inversion between $5f$ and $3d$ levels in Li-like Al XI, and a gain-length product of 2–2.5 between those levels has been reported. More recently, Jaeglé and his group, in experiments in collaboration with the Rutherford-Appleton Laboratory also measured gain for the $4f$–$3d$ transition in Li-like Al XI, using a C fiber coated with a thin layer of Al.[15] At Princeton University, early investigations of Li-like spectra have also shown evidence of population inversions between the $3d$ and $4f$ levels in O VI and Ne VIII,[16,17] with an estimated gain of 1.8 cm^{-1} for the case of O VI.

In the recombination scheme a powerful laser is focused onto a solid target, creating a large population of ions in an ionization stage above the one in which a population inversion between excited levels is desired, i.e., He-like ions for a population inversion in Li-like ions. Then, rapid cooling after the laser pulse by radiation (impurities are added to increase the radiative cooling) and the maintenance of a high electron density of $n_e \sim 5 \times 10^{18}$ cm^{-3} by the magnetic field make favorable conditions for a population inversion between two low-lying excited levels such as $4f$ and $3d$ levels in Li-like ions. At a relatively low electron temperature and high electron density, three-body recombination followed by cascading processes dominates collisional ionization and excitation processes, populating the upper level ($4f$) while the lower level ($3d$) decays rapidly by its strong radiative transition. In this way a population inversion between two excited levels is created.

An important feature in Li-like ions is the fast radiative transition of the $3d$ level to $2p$ due to the large overlap of the radial wave functions of those levels, so that the $3d$ level is rapidly depopulated during the recombination phase, permitting a population inversion to build up. Another merit of Li-like ions is a lower ionization potential than H-like ions with a comparable lasing wavelength. For example, Si XII has an ionization potential of 523 eV for a $4f$–$3d$ transition at 129 Å, compared with H-like N VII, which has an ionization potential of 667 eV for a 3–2 transition at 134 Å. However, for a given plasma electron density, such as may be limited to approximately 1×10^{19} cm^{-3}, which is the critical density for the CO_2 laser, the ion density of Si XII is lower than that of N VII. The trade-off between these and other factors is a subject of theoretical and experimental investigations.

In Section 2 we discuss the main features of the one-dimensional Lagrangian hydrodynamic code and the atomic in Eq. (3) is the energy equilibration time between electrons

0740-3224/89/010115-11$02.00

physics code applied to the modeling of time development of the gain in the recombining Li-like plasma. In Section 3 the experimental setup and results are presented and compared with theoretical calculations.

2. THEORETICAL MODEL

A. Hydrodynamic Model

In this section we discuss the basic features of the one-dimensional hydrodynamic model,[18] which was developed to provide insight into the behavior of the magnetically confined, laser-produced C plasma used in the 182-Å soft-x-ray laser. One of the first hydrodynamic computer codes was developed at the Naval Research Laboratory and was used to study the laser-produced plasmas.[19] A more detailed description of this model will be published elsewhere. The hydrodynamic code with atomic data on the experimental species (in our case Al or Si) and the atomic physics code (discussed below) for Li-like ions permitted us to simulate experiments with Li-like ions.

The basic equations to be solved for a cylindrical plasma are presented here. The continuity equation is given by

$$\frac{\partial n_i}{\partial t} + \frac{1}{r}\frac{\partial}{\partial r}(r n_i v) = \delta_i + \frac{1}{r}\frac{\partial}{\partial r}\left(Dr\frac{\partial n_i}{\partial r}\right), \tag{1}$$

where n_i is the population of the ground state of the ith ionization stage, v is the mean fluid velocity, and δ_i is given by

$$\delta_i = -n_e n_i R_i - n_e n_i S_i + n_e n_{i+1} R_{i+1} + n_e n_{i-1} S_{i-1},$$

where S is the collisional ionization rate from the ground state of the ith ionization stage[20] and R_i represents the collisional dielectronic recombination coefficient of Summers.[21,22] Summers has calculated this coefficient, taking into account recombinations to and ionizations from excited and ground states. Recombination to and ionization from neutrals are neglected because we are interested in a high ionization stage, e.g., Al^{10+}. The second term on the right-hand side of Eq. (1) takes into account the ion–ion diffusion process. The transport of He-like Al XII from the central laser-heated region to the off-axis cold region where they recombine into Li-like ions is crucial to the generation of high gain. Figure 1 shows the variation of the maximum gain for the $4f$–$3d$ transition in Li-like Al XI and the radial position where the maximum gain occurs with different values of the diffusion coefficient. This was generated with the laser input energy kept constant. $D = 5 \times 10^4$ cm^2/sec was chosen throughout the calculations because it produces the highest gain at the proper position observed experimentally.[2] This value is several orders of magnitude higher than the classical diffusion coefficient at $T_i \simeq 100$ eV and $n_e \simeq 1 \times 10^{18}$ cm^{-3}. To understand this discrepancy requires an investigation of diffusion processes in the laser-produced dense plasma, which is beyond the scope of the present paper.

The equation of motion is

$$Mn\left(\frac{\partial v}{\partial t} + v\frac{\partial v}{\partial r}\right) + \frac{\partial}{\partial r}[k(n_e T_e + n T_i) + Q] = -\frac{B}{4\pi}\frac{\partial B}{\partial r}, \tag{2}$$

where M is the ion mass, n is the total ion density, $n = \sum_i n_i$, k is the Boltzmann constant, T_e and T_i are the electron and ion temperature, respectively, and B is the magnetic field strength. Q denotes the artifical viscosity term to handle the shock wave due to the strong expansion[23]:

$$Q = \begin{cases} AMn\left(\dfrac{\partial v}{\partial r}\right)^2 & \text{if } \dfrac{\partial v}{\partial r} < 0 \\ 0 & \text{if } \dfrac{\partial v}{\partial r} > 0 \end{cases}$$

where A is a constant and is chosen in such a way that no numerical instabilities take place because of the propagation of a shock wave.

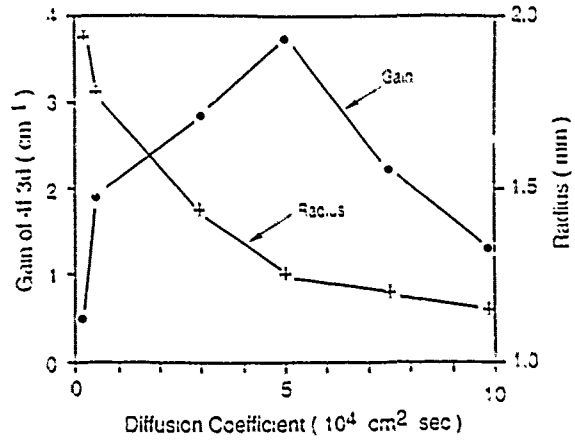

Fig. 1. The maximum gain and its position versus the diffusion coefficient with laser input energy and amount of impurity (Fe) kept constant. filled circles, the maximum gain of the $4f$–$3d$ transition in Li-like Al XI, crosses, the radial position where the maximum gain occurs. Lines are drawn between points as a visual aid.

Laser radiation is absorbed by electrons, and electrons exchange their energy with ions at the classical equipartition rate. It is assumed that the shock wave heats ions only and that the electrons behave adiabatically. Then, the electron temperature is given by

$$\frac{\partial T_e}{\partial t} + v\frac{\partial T_e}{\partial r} = -\frac{2}{3}T_e\frac{1}{r}\frac{\partial}{\partial r}(rv) + \frac{2}{3}\frac{1}{n_e}\frac{1}{r}\frac{\partial}{\partial r}\left(\kappa_e r\frac{\partial T_e}{\partial r}\right) + \frac{2}{3}\frac{\epsilon_J}{n_e} - \frac{T_e - T_i}{\tau_{eq}} + \frac{2}{3}\frac{\epsilon_L}{n_e} - \frac{2}{3}P_{atom}, \tag{3}$$

where κ_e is the electron thermal conductivity divided by the Boltzmann constant k, terms on the right-hand side represent work done on expansion, thermal conduction losses, and ohmic heating due to the induced current, energy transfer to ions, and laser energy input, respectively, and the last term is energy losses by atomic processes:

$$P_{atom} = P_{rad} + P_{ionization} - P_{recombination} + P_{impurity}.$$

Here P_{rad} denotes the total energy loss by resonant radiations following collisional excitations, $P_{ionization}$ is the total energy loss by ionization processes, $P_{recombination}$ is the total energy recovery by recombination processes, and $P_{impurity}$ is the total energy loss by an impurity (Fe in our calculation). The ohmic heating term is defined by the plasma resistivity η as $\epsilon_J = [c^2\eta/(4\pi)^2](\partial B/\partial r)^2$, where c is the speed of light, τ_{eq}

and ions, and ϵ_L is the power per unit volume absorbed by electrons from the laser. Impurities are assumed to be distributed uniformly. Data for the electron cooling rate of Fe in a dense, transient plasma are not available. As a first approximation, we have used the radiation cooling rates of Post *et al.*[24] for a steady-state coronal plasma. At high electron densities, the radiation cooling coefficient per electron per ion is reduced because of the decrease of energy loss through $\Delta n = 0$ transitions as a result of the increase of collisional deexcitation rates.[25] Figure 2 shows the reduction factor of the radiation cooling coefficient per electron per ion, $1 + n_e S_{lm}^{II}/A_{lm}$, versus the electron temperature for $\Delta n = 0$ transitions in Fe at given electron densities. S_{lm}^{II} and A_{lm} are collisional deexcitation and radiative transition rates, weight averaged over the possible allowed $\Delta n = 0$ transitions. Expressions by Post *et al.*[24] in an average-ion model were used for S_{lm}^{II} and A_{lm}. At the condition when $T_e = 5$ eV and $n_e \simeq 4 \times 10^{18}$ cm^{-3}, the radiation cooling rate of Post *et al.* would be reduced by approximately 1 order of magnitude. More-complete calculation of the cooling rate by Fe in the high electron densities above the coronal limit is planned by using an average-ion model. Results with the present code, however, are in reasonable agreement with experimental data, as is discussed in Section 3.

The ion temperature is governed by

$$\frac{\partial T_i}{\partial t} + v\frac{\partial T_i}{\partial r} = -\frac{2}{3}\left(T_i + \frac{Q}{n}\right)\frac{1}{r}\frac{\partial}{\partial r}(rv) + \frac{2}{3}\frac{1}{n}\frac{1}{r}\frac{\partial}{\partial r}\left(\kappa_i r\frac{\partial T_i}{\partial r}\right) + \frac{T_e - T_i}{\tau_{eq}}. \quad (4)$$

The first term on the right-hand side includes the heating by the shock wave. κ_i is the ion thermal conductivity divided by the Boltzmann constant k. Expressions by Braginskii[26] are used for κ_e and κ_i.

Finally, the equation for the magnetic field is given by

$$\frac{\partial B}{\partial t} + v\frac{\partial B}{\partial r} = -\frac{B}{r}\frac{\partial}{\partial r}(rv) + \frac{1}{r}\frac{\partial}{\partial r}\left(\frac{c^2}{4\pi}\eta r\frac{\partial B}{\partial r}\right). \quad (5)$$

A Lagrangian scheme has been adopted to solve Eqs. (1)–(5). The difference equations are written in such a way that Eqs. (1), (3), (4), and (5) are treated implicitly, and Eq. (2) is treated explicitly.[23] The spatial grid structure has 30 grid points, and the final grid point was taken to be at 5 mm, with the grid size increasing exponentially from a minimum size of 20 μm at the center. In this way we can preserve as much detail as possible near the central region, which we are interested in, and use the computer CPU time more efficiently.

The plasma outer radius R_0 (5 mm in calculation) is much larger than the central region (which is typically within a 1.5-mm radius). The boundary conditions are

$$T_{e,i} \to T_0, \quad B \to B_0, \quad v \to v_0, \quad \text{as } r \to R_0,$$

and at the origin

$$\frac{\partial T_{e,i}}{\partial r} \to 0, \quad \frac{\partial B}{\partial r} \to 0, \quad \frac{\partial v}{\partial r} \to 0 \quad \text{as } r \to 0.$$

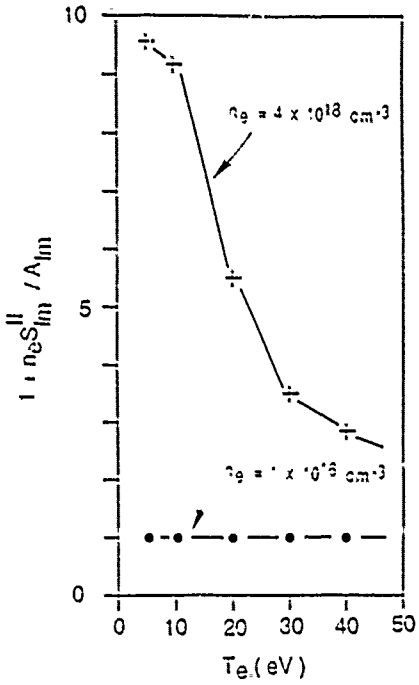

Fig. 2. The variation of the reduction factor, $1 + n_e S_{lm}^{II}/A_{lm}$, of the radiative cooling rate per ion per electron with respect to the electron temperature at given electron densities. In low electron densities (filled circles) the factor approaches unity, but in high electron densities (crosses) and low electron temperature, $\Delta n = 0$ collisional deexcitation rates dominate $\Delta n = 0$ radiative transition rates, resulting in the reduction in the cooling rate. This calculation was done for Fe by using the average-ion model used by Post *et al.*[24] Lines are drawn as a visual aid.

The initial electron temperature profile is set to be Gaussian with $T_{e,max} = 20$ eV and $T_{e,min} = 3$ eV. Then, profiles of total ion density, magnetic field, steady-state ionization balance, and electron density are determined by using the local pressure balance. During the time development from the plasma described above, the hydrodynamic code calculates, at each time step, various hydrodynamic parameters from which electron temperature, electron density, and ground-state population of Li- and He-like ions are input to a post-processor atomic physics code in order to calculate populations of excited levels and generate line intensities and gains of various transitions in Li-like Al XI.

B. Excited States in the Lithiumlike Ion

The level structure considered and relevant transitions in the atomic physics code are shown in Fig. 3. Seventy-seven levels up to the principal quantum number equal to 12 were included. A population inversion between the $4f$ and $3d$ levels is expected for the plasma conditions when the electron temperature and density are $T_e \simeq 10$ eV and $n_e \simeq 5 \times 10^{18}$ cm^{-3}. In this region levels above $n = 5$ (n is the principal quantum number) are in local thermal equilibrium (LTE) with the ground state of He-like ions,[27] and their populations are calculated from the Saha–Boltzmann equation. Populations of excited levels from $n = 2$ to $n = 5$ are calculated by using the following collisional-radiative model.

We solve the following coupled rate equation:

$$\frac{d}{dt} n_{q,l} = n_e \sum_{m=l+1}^{k_{max}} (n_{q,m} S_{m,l}^{II} - n_{q,l} S_{l,m}^{I})$$

$$+ n_e \sum_{m=1}^{l-1} (n_{q,m} S_{m,l}^{I} - n_{q,l} S_{l,m}^{II})$$

$$- n_e \sum_{m=1}^{l-1} A_{l,m} + \sum_{m=l+1}^{k_{max}} n_{q,m} A_{m,l}$$

$$- n_e n_{q,l} S_{q,l} + n_{q+1} n_e^2 (\alpha_{q,l} + n_e \beta_{q,l}), \quad (6)$$

where $n_{q,l}$ denotes the population of an excited level l in the ionization stage q, n_{q+1} is the population of the ground state of the ionization stage $q + 1$, $S_{l,m}^{I}$ and $S_{l,m}^{II}$ are the collisional excitation and deexcitation rate between levels l and m, respectively, $\alpha_{q,l}$ and $\beta_{q,l}$ are the radiative and three-body recombination rates, respectively, k_{max} is the highest level considered (see Fig. 3), $A_{l,m}$ is the spontaneous emission rate between levels l and m, and $S_{q,l}$ is the collisional ionization rate from level l.

As discussed by Bates *et al.*,[28] relaxation of the excited levels is much more rapid than that of the ground level at the densities currently considered. Thus the left-hand side of Eq. (6) can be set to zero, and the calculation of populations of excited levels for given populations of ground states of adjacent ionization stages becomes an inversion of a matrix whose elements are composed of various rates between the levels:

$$\mathbf{n}_q = -\mathbf{E} \cdot \tilde{\mathbf{C}}^{-1}, \quad (7)$$

where

$$C_{l,m} = \begin{cases} n_e S_{m,l}^{II} + A_{m,l} & m > l \\ -\left[n_e \sum_{k=l+1}^{k_{max}} S_{l,k}^{II} + \sum_{k=1}^{l-1} (n_e S_{l,k}^{II} + A_{l,k}) + n_e S_{q,l}\right] & m = l \\ n_e S_{m,l}^{I} & m < l \end{cases}$$

$$E_l = n_e n_{q+1} (\alpha_{q,l} + n_e \beta_{q,l}) + n_e n_{q,l} S_{1,l}^{I}$$

$$+ \sum_{k=n_{max}+1}^{k_{max}} n_k (n_e S_{k,l}^{II} + A_{k,l}),$$

and $2 < l, m < n_{max}$, where n_{max} is the last level in the collisional-radiative model (see Fig. 3).

The atomic data on various atomic processes used in the solution of the coupled rate equation for populations of excited levels come from a variety of sources. Energy levels and radiative transition rates were taken from the work of Lingård and Nielson.[29] For collisional excitation $2s$–nf (n = 4, 5, 6), the literature of Petrini was used,[30] and for $2p$–ns, $2p$–np, and $2p$–nd ($n \geq 2$), rates of Bely and Petrini were used.[31] The remaining electron collisional excitation rates were estimated from the interpolation formulas by Mewe.[32] An expression for collisional ionization rates from excited states by Post *et al.*[24] was adopted, and the three-body recombination to excited levels and the collisional deexcitation rates were estimated by the principle of detailed balance. Only ionization from an excited level to the ground

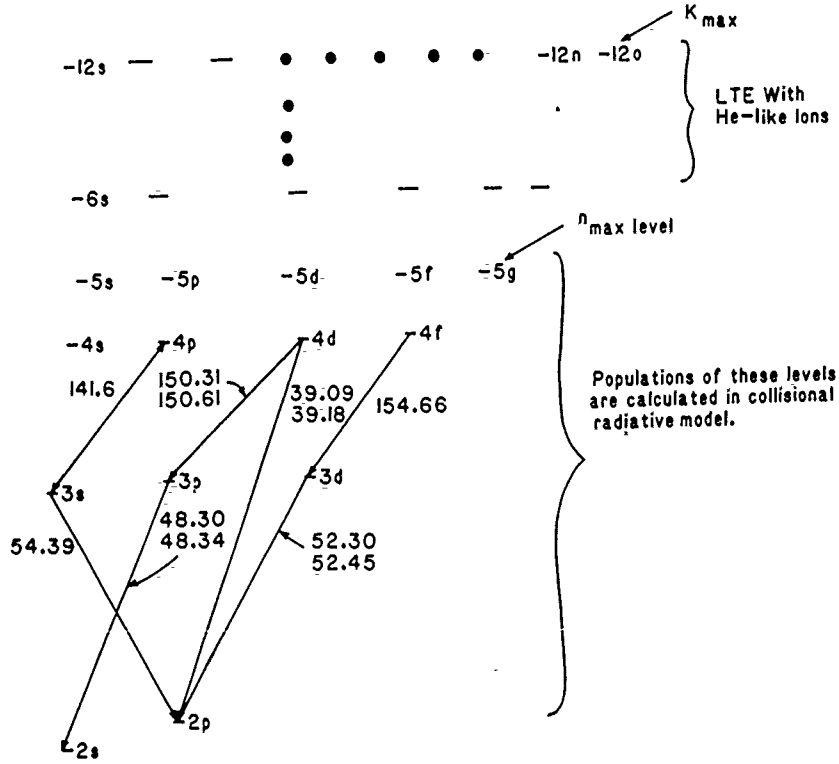

Fig. 3. Grotrian diagram of Li-like Al. Populations of levels between n = 6 and n = 12 are calculated through local thermodynamic equilibrium with He-like ions.

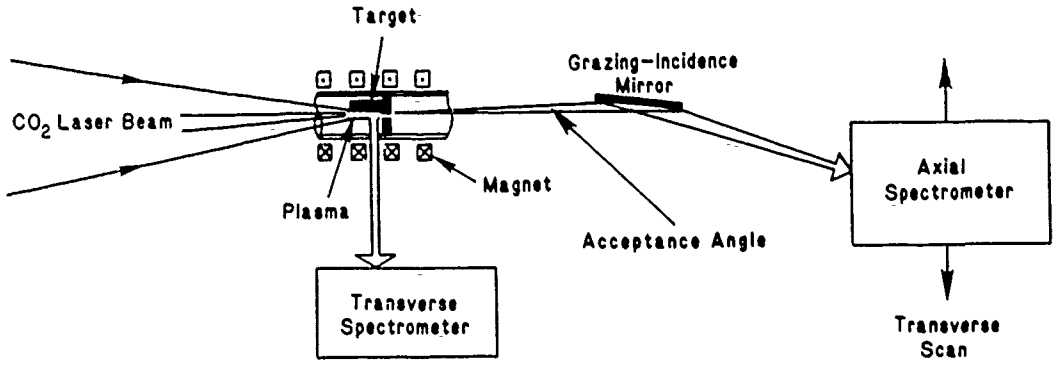

Fig. 4. Experimental setup.

state in the next higher ionization stage was considered. The radiative recombination rates of Burgess for H-like ions was used. Dielectronic recombination processes were not included in our calculation because these processes are expected to be negligible compared with three-body recombination processes under the conditions that we are interested in.

The plasma is assumed to be optically thin. The $3d$–$2p$ transition is the most absorbable because its gA value (g is the statistical weight and A is the spontaneous emission rate) is large, and the populations of $2p$ levels is much greater than those of the excited levels. However, even for the $3d$–$2p$ transition of Li-like ions in the transverse spectra, the plasma in our experiment is observed to be optically thin in the transverse direction (as discussed in Section 3).

With populations of excited states calculated as described above, gains at the line center for $4f$–$3d$, $4d$–$3p$, and $4p$–$3s$ transitions and line intensities of various transitions shown in Fig. 3 are calculated. The gain per unit length G for a transition between levels l and m is given by

$$G(\lambda_{lm}) = \frac{1}{8\pi c}\frac{\lambda_{lm}^4}{\Delta\lambda} g_l A_{lm}\left(\frac{N_l}{g_l} - \frac{N_m}{g_m}\right)(\mathrm{cm}^{-1}), \qquad (8)$$

where λ_{lm} is the wavelength of the l–m transition and $\Delta\lambda$ is the linewidth. For the condition of maximum gain presented below, Stark broadening due to the electron impact was smaller than the Doppler broadening by a factor of 2. Therefore for simplicity we have assumed that the Doppler broadening is dominant and $T_i \simeq T_e$ for $T_e \leq 50$ eV throughout the gain calculation.

After the calculation of gains and line intensities as a function of space and time, the axial and transverse spectra for comparisons with experimental data were generated by integrating the intensity of each line over the spatial region viewed by the axial and transverse spectrometers, respectively, and then over time. The amplification by stimulated emission, $(e^{GL}-1)/GL$, in the axial spectrum was taken into

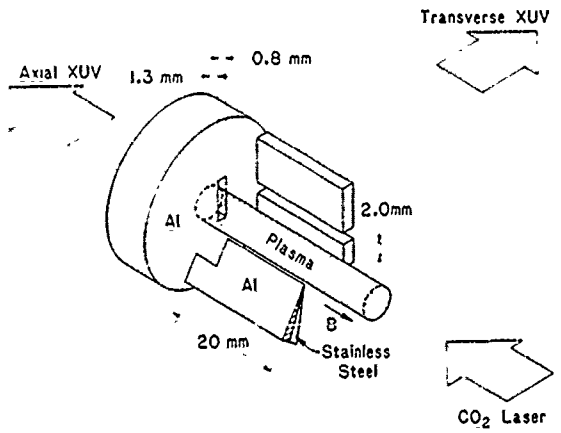

Fig. 5. An Al disk target geometry with a 0.8 mm × 2 mm vertical slot and an Al–stainless steel composite blade attached perpendicular to the target surface.

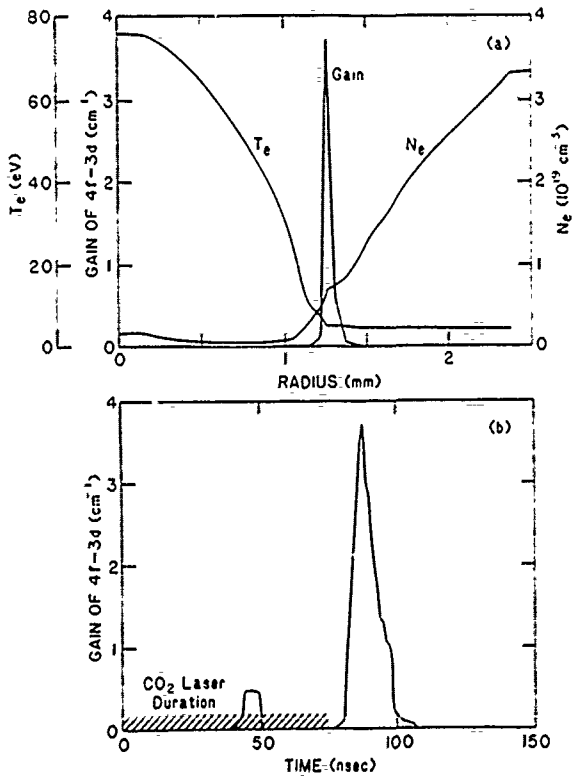

Fig. 6. (a) Calculated radial profiles of electron density, electron temperature, and gain for the $4f$–$3d$ transition (154 Å) at the time of maximum gain in Li-like Al XI. (b) The time history of the gain for the $4f$–$3d$ transition in Li-like Al XI at a radial position 1.2 mm off axis.

account. L is the plasma length, which was taken to be 1 cm, as observed in an earlier experiment.[14]

3. EXPERIMENTAL RESULTS AND THEIR COMPARISON WITH CALCULATION

The experimental setup is shown in Fig. 4. A CO_2 laser (~500 J) is focused onto an Al or Si target and creates a highly ionized plasma column confined in a strong axial magnetic field. The maximum laser power density on the target is 2×10^{11} W/cm^2. A composite blade made from a sandwich of Al and stainless steel (or Si and Ti for Si targets) is attached perpendicularly to the target surface (see Fig. 5). The plasma is viewed in both axial and transverse directions by multichannel soft-x-ray spectrometers,[15] which produce time-integrated spectra. The target design is based on the C target, which was used to generate lasing action at C VI 182 Å.[7] Previous research with C targets showed improved axial uniformity when blades were incorporated into the target. Measurement of the chordal brightness of Si XII 129-Å line in the transverse direction with the present target (shown in Fig. 5) suggested good radial symmetry. Also the blade provides a way to introduce impurities (stainless steel or Ti in our experiment) for additional cooling.

Theoretical radial profiles of the electron temperature, the electron density, and the gain at the time when the gain reaches its maximum in Li-like Al XI are shown in Fig. 6(a). The input laser pulse used in the calculation has a Gaussian shape with the FWHM of 50 nsec and a falling time of 60 nsec. (The real laser pulse has a FWHM of 50–60 nsec and a falling time of 70–80 nsec.) Fe was included as an impurity to provide additional cooling. The center of the plasma is heated directly by the laser, and a shock wave is generated that transports ions away from the central hot region, producing favorable conditions for the gain at 1–1.5 mm off axis. Figure 6(b) shows the theoretical time history of the gain for the $4f$–$3d$ transitions at a radial position 1.2 mm off axis. The gain peaks at 87 nsec from the beginning of the laser pulse and has a duration of approximately 20 nsec in this particular run. The double-pulse structure is explained as follows. During the laser pulse, He-like ions created in the central hot region diffuse into the region that is 1.2 mm away from the center and still cold. Here they recombine into Li-like ions and produce the first population inversion. As the laser continues to heat plasma, this off-axis region is heated, and gain disappears. High gain, however, occurs again at approximately 90 nsec from the beginning of the CO_2 laser pulse, as the temperature and density conditions are more appropriate.

Figure 7 shows experimental transverse spectra along with

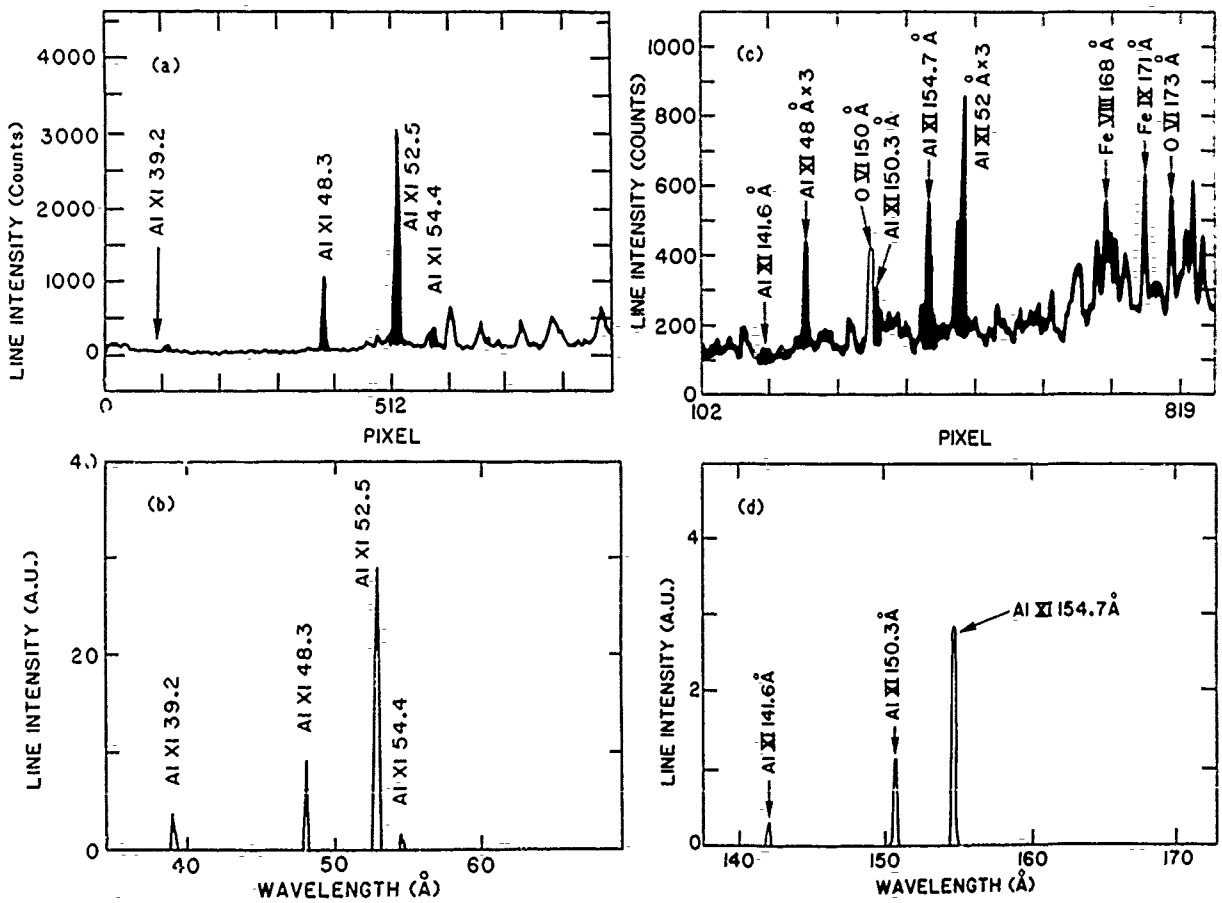

Fig. 7. (a), (c) Plasma emissions recorded by the transverse spectrometer in the spectral ranges of 30–60 and 140–170 Å, respectively. (b), (d) Calculated transverse emission spectra in the spectral ranges 30–60 and 140–170 Å, respectively. The linewidths in the theoretical spectra do not have any physical meaning. $B = 70$ kG were used in both experiment and computer simulation.

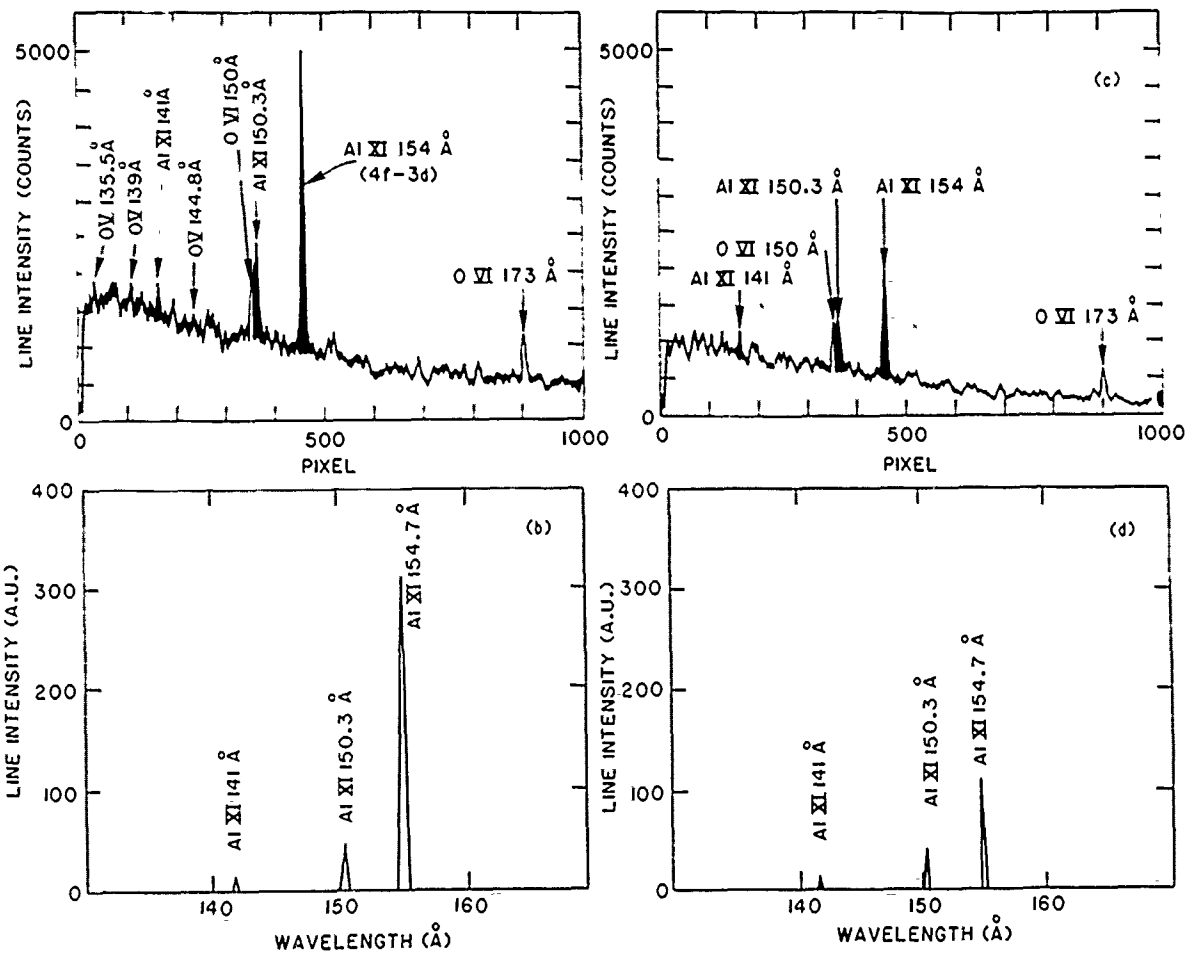

Fig 8. Axial spectra in the spectral region of 140–170 Å. (a) and (c), recorded by the axial spectrometer for the gain and the nongain region, respectively. (b) and (d), calculated time-integrated axial spectra over the gain region and the nongain region, respectively. B = 70 kG were used in both experiment and computer simulation.

theoretically calculated transverse spectra for comparison. In the spectral region of 140–170 Å, line ratios between 141.6, 150.3, and 154.7 Å in the experimental spectra [Fig. 7(c)] are in good agreement with those predicted theoretically [Fig. 7(d)]. Note that in Fig. 7(c) the line intensity ratio of the third order of the 52.3- and 52.45-Å lines, which make up the $3d$–$2p$ transition doublet, is 2:1. When we consider that the ratio of gA values of this doublet is 2:1 and that this transition is the most absorbable, this observation indicates that the plasma is optically thin in the transverse direction for the transitions shown in Fig. 3. This is important as it permits the Al XI 52.4-Å line to depopulate the $3d$ level efficiently and to generate a population inversion. Also, in the wavelength region of 30–60 Å [Figs. 7(a) and 7(b)], reasonable agreement between experimental and theoretical spectra is observed except for the 39.2-Å line, $4f$–$2p$ transition. This discrepancy may be due to a change of sensitivity of the detector in the short-wavelength region.

The axial emission is imaged by a grazing-incidence mirror onto the entrance slit of a multichannel soft-x-ray spectrometer, as shown in Fig. 4. The mirror is constructed by bending a glass strip; thus the optical quality of the system is not ideal. However, a transverse scan of the axial spectrometer allows us to view different ~200-μm-wide plasma regions. By changing the transverse position of the axial spectrometer, the geometry of the present experimental setup (the small acceptance angle, 1.6 mrad, by the grazing-incidence mirror) allows us to adjust the spectrometer to view the region with high gain (we refer to this region as the gain region) or the region with little or no gain (we refer to this region as the nongain region). On the spectrum recorded from the gain region, we expect to see the amplification of the potential lasing line by stimulated emission. This effect was clearly shown in the work on H-like C VI, where extensive observations of absolute intensity and measurements of absolute divergence were the primary evidence for lasing.[6]

Figures 8(a) and 8(c) show the spectra recorded by the axial spectrometer at the two different transverse positions of the spectrometer. At one position the intensity of the Al XI 154 Å is significantly increased, whereas intensities of other transitions remain almost constant. The ratio of the line intensity of the Al XI 154-Å ($4f$–$3d$) to that of the Al XI 141-Å ($4p$–$3s$) line is three times higher in the gain-region spectrum [Fig. 8(a)] than in the nongain-region spectrum [Fig. 8(c)]. Gain-region and nongain-region spectra including the effect of stimulated emission were generated theoretical-

ly by changing the spatial region over which the intensity of each line was integrated. The computer code models a 1-cm-long, cylindrically symmetric plasma and predicts an annulus gain region that is approximately 100 μm wide (see Fig. 6). In the experiment the axial spectrometer views a rectangular plasma region ~200 μm wide. For the calculated gain region spectrum, a 200 μm × 2 mm region of the computer-generated plasma was chosen to include the high-gain region, and the intensity of each line was integrated spatially over that region and then over time. For the non-gain-region spectrum, the integration region did not include the gain region. As observed in the experimental spectra, the ratio of the 154- to 141-Å line intensity is approximately three times larger in the calculated gain-region spectrum [Fig. 8(b)] than in the calculated nongain-region spectrum [Fig. 8(d)] for the model plasma, which has a gain-length product GL = 3.7. The difference of a factor of 1.7 in the ratio of the line intensity of 154 to 141 Å between experimental and theoretical spectra could be due to the variation of spectrometer detector sensitivity with wavelength, which has, of course, no effect on present results for relative values of line intensities for the gain and the nongain region.

Comparison of the axial spectrum in the spectral region of 30–60 Å between experiment and calculation is shown in Fig. 9. The experimental spectra, Figs. 9(a) and 9(b), correspond to the nongain-region and the gain-region spectra, respectively. Theoretical spectra were produced by integrating each line over the nongain region [Fig. 9(c)] and the gain region [Fig. 9(d)], as in Fig. 8. Estimation from Eq. (8) shows that at conditions of $T_e \cong 5.0$ eV and $n_e \cong 3 \times 10^{19}$ cm^{-3} the optical depth of the 52.3-Å resonance line is approximately 300 μm, which is quite small compared with the axial length of the plasma, 1 cm. Because of the strong self-absorption of the 52.3-Å resonance line in the axial direction, comparisons involving the 52.3-Å line are of limited value because the present code does not account for opacity. There is, however, one interesting observation that the ratio of intensities of the 48.3-Å line ($3p$–$2s$ transition) to 54.4-Å

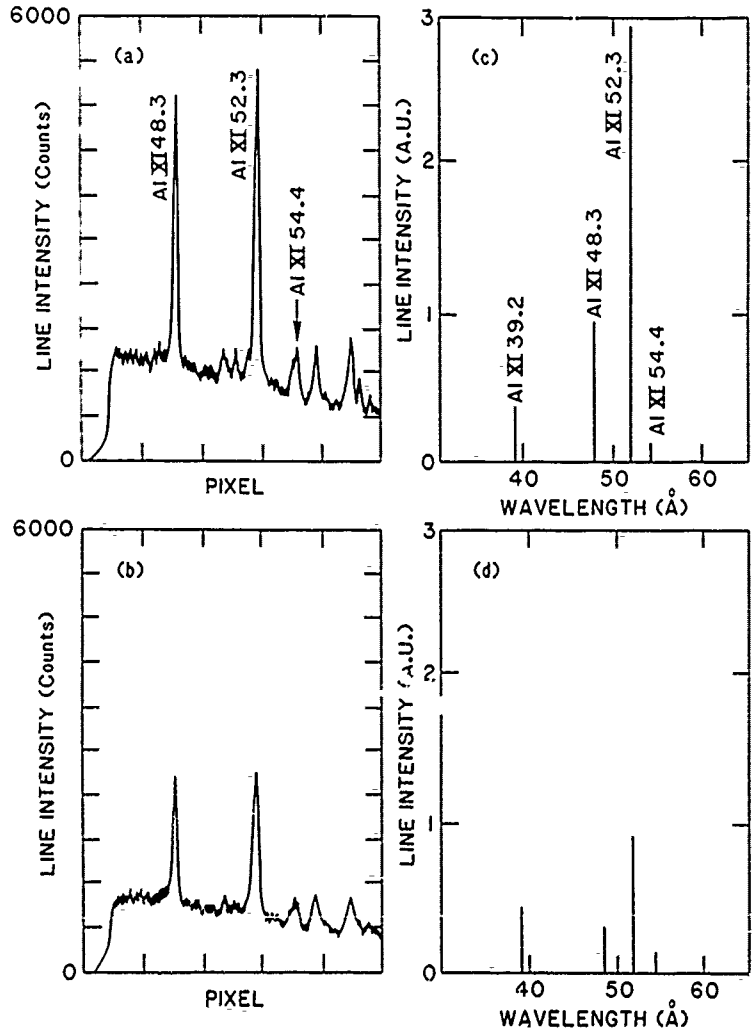

Fig. 9. Axial spectra in the spectral region of 30–60 Å. (a) and (b), recorded by the axial spectrometer for the nongain and gain regions, respectively. (c) and (d), calculated time-integrated axial spectra over the nongain region and the gain region, respectively. B = 70 kG were used in both experiment and computer simulation.

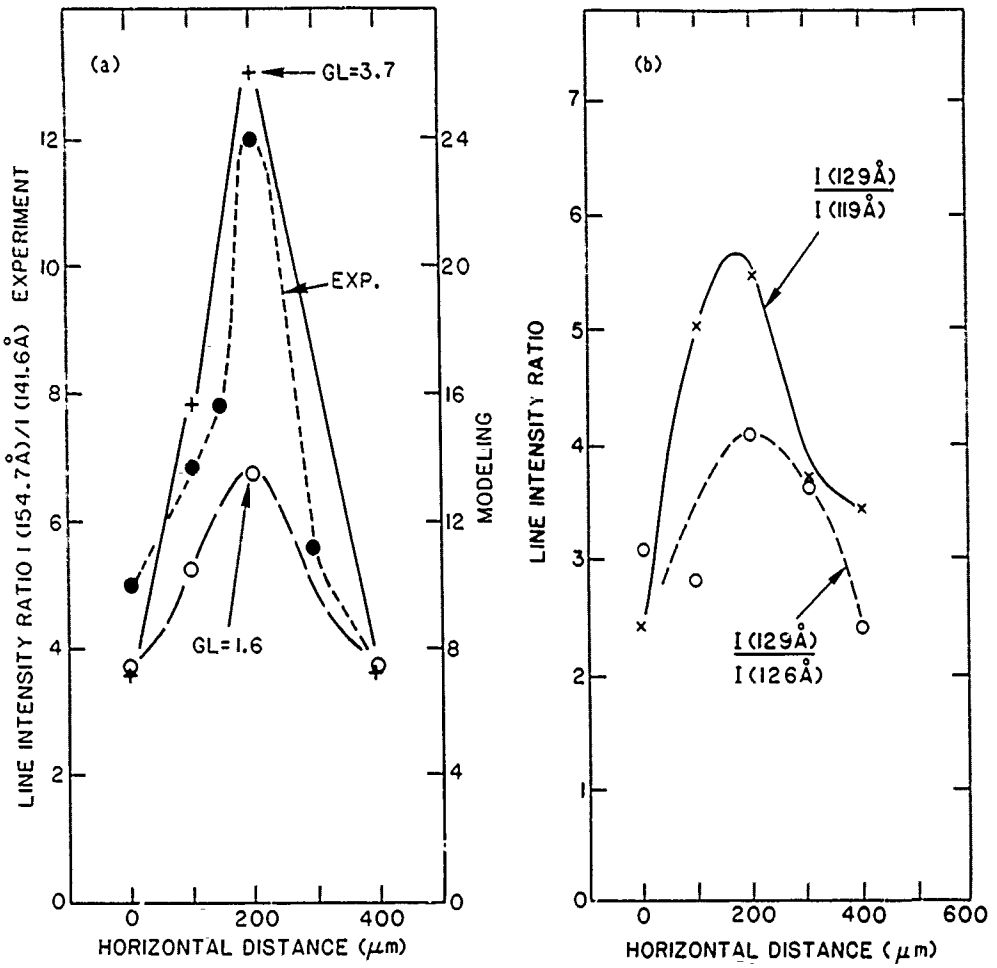

Fig. 10. (a) Observed and predicted line intensity ratio versus horizontal position of the axial spectrometer showing the rise in relative intensity of the Al XI 4*f*–3*d* transition at 154.7 Å in the region of the plasma with gain. filled circles, experimental data, open circles, modeling with peak gain-length product GL = 1.6, crosses, modeling with peak gain-length product GL = 3.7. (b) The line ratios of Si XII 129 to 119 Å and Si XII 129 to 126 Å are shown as a function of the transverse position of the axial spectrometer.

line (3*s*–2*p* transition) changes from 6.5 in the nongain region [Fig. 9(c)] to 2.5 in the gain region [Fig. 9(d)]. This trend can also be seen in experimental spectra [Figs. 9(a) and 9(b)]. The ratio of the 48.3-Å line to the 54.4-Å line in Fig. 9(a) is 6.0, and that in Fig. 9(b) is 4.2. This indicates that the population of the 3*p* level relative to that of the 3*s* level in the gain region is lower than it is in the nongain region. We believe that the reason is that the temperature of the gain region is ~5 eV, as seen in Fig. 6(a), and at such temperatures the deexcitation process between 3*p* and 3*s* becomes dominant over the excitation process, resulting in a decrease in the 3*p* level population. Another observation is that, in general, line intensities in Figs. 9(b) and 9(d) (the gain region) are about one third of those in Figs. 9(a) and 9(c) (the nongain region). The main reason for this is that our experimental and calculated spectra are time integrated and include emission from both the ionization and recombination phases; emissions during the ionization phase in the nongain region make significant contributions to the nongain-region time-integrated spectra because in this region the electron temperature becomes high (~150 eV) enough to have $n = 3$ levels much populated through collisional excitation processes, whereas the gain region never reaches a high electron temperature and dominant contributions to the gain-region spectra come during the recombination phase.

A convenient way of showing the amplification of the 4*f*–3*d* transition is to measure the line intensity of this transition relative to that of the 4*p*–3*s* transition. This comparison, being based on lines in the same ion from upper levels with the same principal quantum number, is independent of uncertainties in the exact spatial distribution of different kinds of ions viewed by the spectrometer. The experimentally observed change in the ratio of the 154- to 141-Å line intensities with respect to the transverse position of the axial spectrometer is shown in Fig. 10(a) along with computational results. The use of the Al XI 150.3-Å line as a reference was avoided for two reasons. The intensity of the Al XI 150.3-Å line is unfortunately blended by the O VI 150.1-Å line. The relative intensities of O VI lines change with plasma conditions, as shown in Figs. 8(a) and 8(c), and it is difficult to deconvolute the intensity of the Al XI 150.3-Å line. Another reason is the possibility that population inversion between 4*d* and 3*p* levels and, therefore, amplification of the Al XI 150.3-Å line may occur. The computations

were performed for two plasma conditions with peak gain-length products GL = 3.7 and GL = 1.6, respectively. These two conditions were obtained by changing the amount of impurity—Fe in our case—while maintaining a constant laser input energy. The additional cooling due to an effective Fe concentration of 7% at $n_e \simeq 4 \times 10^{18}$ cm^{-3} was modeled by using the coronal data[24] with the Fe concentration set of 0.7% (see Subsection 2.A). This resulted in a peak gain-length product of GL = 3.7. With an effective Fe concentration of 5% (i.e., 0.5% used in the code) the gain-length product was GL = 1.6. Experimentally, impurities are provided by the interaction of plasma with the composite blade of Al and stainless steel. It can be seen that there is good agreement between the shape of the curves for GL = 3.7 and the experimental data.

Similar experimental have been performed with Si XII. In this case the $4f$–$3d$ gain transition is at 129 Å and the neighboring $4d$–$3p$ and $4p$–$3s$ transitions are at 126 Å and 119 Å, respectively. The target configuration was similar to Fig. 5 but with a Si disc and a Si–Ti composite blade. Because the Si XII ionization potential (523 eV) is higher than that of Al XI (442 eV) and the gain wavelength is shorter, it is expected to be more difficult to generate gain in Si XII than in Al XI. Preliminary results are shown in Fig. 10(b), where the relative intensity of the 129-Å line compared with the 126- and 119-Å lines is shown. The peak in the intensity ratios is a clear indication of gain-length product, GL, of order 1–2, and we expect that with further optimization of experimental conditions higher values of gain will be obtained.

4. SUMMARY AND FUTURE PLAN

We have demonstrated the amplification of 154-Å radiation in Al XI and 129-Å radiation in Si XII for transitions between the $4f$ and $3d$ levels in a CO_2 laser-produced recombining plasma confined in a strong axial magnetic field. The maximum gain-length products observed are GL ~ 3–4 for 154 Å in Al XI and GL ~ 1–2 for 129 Å in Si XII.

A one-dimensional hydrodynamic code with a postprocessor atomic physics code was used to simulate the experiment. It was shown that the theoretical spectra are in good agreement with experimental data, even though there are several assumptions in the simulation that simplifies the real situation: a cylindrically symmetric plasma, uniform distribution of impurities, and approximation to the energy loss rate of the impurity in a transient, high-electron-density plasma by scaling steady-state coronal cooling data.

In terms of increasing the power level of the present soft-x-ray laser, a large increase in brightness is potentially possible if a cavity formed by two soft-x-ray mirrors is applied to a high-gain medium. Soft-x-ray mirrors with reflectivities in excess of 40% at 182 Å recently became available, and a cavity formed by two such mirrors combined with a gain medium with a gain-length product of GL > 3 should oscillate, provided that the gain duration is sufficient for several round trips of light between the mirrors (≥10 nsec). A 120% increase in stimulated emission was observed in early experiments by using one mirror of 12% reflectivity in a double-pass configuration,[2,36] but mirror alignment posed severe difficulties. A new experimental setup to overcome these problems has been constructed, and cavity experiments are planned for the near future.

ACKNOWLEDGMENTS

We thank H. Furth for support and stimulating discussions. We also acknowledge help from L. Meixler and technical assistance from A. Schuessler and S. Cranmer. This research was made possible by financial support from the U.S. Department of Energy, Advanced Energy Projects of Basic Energy Sciences, the U.S. Air Force Office of Scientific Research, and the Naval Research Laboratory/Strategic Defense Initiative Office.

S. Suckewer is also with the Department of Mechanical and Aerospace Engineering, Princeton University, Princeton, New Jersey 08543.

REFERENCES

1. D. L. Matthews, P. L. Hagelstein, M. D. Rosen, M. J. Eckart, N. M. Ceglio, A. U. Hazi, H. Medecki, B. J. MacGowan, J. E. Trebes, B. L. Whitten, E. M. Campbell, C. W. Hatcher, A. M. Hawryluk, R. L. Kauffman, L. D. Pleasance, G. Rambach, J. H. Scofield, G. Stone, and T. A. Weaver, Phys. Rev. Lett. 54, 110 (1985).
2. S. Suckewer, C. H. Skinner, H. Milchberg, C. Keane, and D Voorhees, Phys. Rev. Lett. 55, 1753 (1985).
3. B. J. MacGowan, S. Maxon, P. L. Hagelstein, C. J. Keane, R. A. London, D. L. Matthews, M. D. Rosen, J. H. Scofield, and D. A. Walan, Phys. Rev. Lett. 59, 2157 (1987).
4. D. Matthews, M. Rosen, S. Brown, N. Ceglio, D. Eder, A. Hawryluk, C. Keane, R. London, B. MacGowan, S. Maxon, D. Nilson, J. Scofield, and J. Trebes, J. Opt. Soc. Am. B 4, 575 (1987).
5. P. Jaeglé, G. Jamelot, A. Carillon, A. Klisnick, A. Sureau, and H. Guennou, J. Opt. Soc. Am. B 4, 563 (1987), and references therein.
6. S. Suckewer, C. H. Skinner, D. Kim, E. Valeo, D. Voorhees, and A. Wouters, Phys. Rev. Lett. 57, 1004 (1986).
7. C. Chenais-Popovics, R. Corbett, C. J. Hooker, M. H. Key, G. P. Kichn, L. S. Lewis, G. J. Pert, C. Regan, S. J. Rose, S. Sadaat, R. Smith, T. Tomie, and O. Willi, Phys. Rev. Lett. 59, 2161 (1987).
8. H. C. Kapteyn, R. W. Lee, and R. W. Falcone, Phys. Rev. Lett. 57, 2939 (1986).
9. M. H. Sher, J. J. Macklin, J. F. Young, and S. E. Harris, Opt. Lett. 12, 891 (1987).
10. T. N. Lee, E. A. McLean, and R. C. Elton, Phys. Rev. Lett. 59, 1185 (1987).
11. W. T. Silfvast, O. R. Wood II, J. J. Macklin, and H. Lundberg, in *Laser Techniques in the Extreme Ultraviolet*, S. E. Harris and T. B. Lucatorto, eds., AIP Conf. Proc. 119, 427 (1984).
12. C. W. Clark, M. G. Littman, R. Miles, T. J. McIlrath, C. H. Skinner, S. Suckewer, and E. Valeo, J. Opt. Soc. Am. B 3, 371 (1986).
13. M. Duguay and A. Rentzepis, Appl. Phys. Lett. 10, 350 (1967).
14. E. J. McGuire, Phys. Rev. Lett. 35, 844 (1975).
15. P. Jaeglé, Laboratoire de Spectroscopie Atomique et Ionique, Université Paris-Sud, Bâtiment 350, 91405 Orsay, France, and M. Key, Rutherford-Appleton Laboratory, Chilton, Didcot, Oxfordshire OX11 0QX, England (personal communication).
16. S. Suckewer, C. Keane, H. Milchberg, C. H. Skinner, and D. Voorhees, in *Laser Techniques in the Extreme Ultraviolet*, S. E. Harris and T. B. Lucatorto, eds., AIP Conf. Proc. 119, 55 (1984).
17. H. Milchberg, J. L. Schwob, C. H. Skinner, S. Suckewer, and D. Voorhees, in *Laser Techniques in the Extreme Ultraviolet*, S. E. Harris and T. B. Lucatorto, eds., AIP Conf. Proc. 119, 379 (1984).
18. E. Valeo, C. Keane, and R. M. Kulsrud, Bull. Am. Phys. Soc. 30, 1600 (1985).
19. P. G. Burkhalter, M. J. Herbst, D. Duston, J. Gardner, M. Emery, R. R. Whitlok, J. Grun, J. P. Apruzese, and J. Davis, Phys. Fluids 26, 3650 (1983), and references therein.
20. R. W. P. McWhirter, in *Plasma Diagnostic Techniques*, R. H. Huddlestone and S. L. Leonard, eds. (Academic, New York, 1965), p. 205.
21. H. P. Summers, Mon. Not. R. Astron. Soc. 169, 663 (1974);

Rutherford-Appleton Laboratory Rep. IM367 (Rutherford-Appleton Laboratory, Chilton, England, 1974).
22. H. P. Summers, Comments At. Mol. Phys. 14, 147 (1984).
23. R. D. Richtmyer and K. W. Morton, *Difference Methods for Initial Value Problems* (Interscience, New York, 1957).
24. D. E. Post, R. V. Jensen, C. B. Tarter, W. H. Grasberger, and W. A. Lokke, At. Data Nucl. Data Tables 20, 397 (1977).
25. C. Keane and C. H. Skinner, Phys. Rev. A 33, 4179 (1986).
26. S. I. Braginskii, in *Reviews of Plasma Physics*, M. A. Leontovich, ed. (Consultants Bureau, New York, 1965), Vol. 1, p. 205.
27. R. Wilson, J. Quant. Spectrosc. Radiat. Transfer 2, 477 (1962).
28. D. R. Bates, A. E. Kingston, and R. W. P. McWhirter, Proc. R. Soc. (London) Ser. A 267, 297 (1962).
29. A. Lingard and S. E. Nielson, At. Data Nucl. Data Tables 19, 533 (1977).
30. D. Petrini, Astron. Astrophys. 17, 410 (1972).
31. O. Bely and D. Petrini, Astron. Astrophys. 6, 318 (1970).
32. R. Mewe, Astron. Astrophys. 20, 215 (1972).
33. A. Burgess, Mem. R. Astron. Soc. 69, 1 (1965).
34. C. H. Skinner, C. Keane, H. Milchberg, S. Suckewer, and D. Voorhees, in *Laser Techniques in the Extreme Ultraviolet*, S. E. Harris and T. B. Lucatorto, eds., AIP Conf. Proc. 119, 372 (1984).
35. J. L. Schwob, A. Wouters, and S. Suckewer, Rev. Sci. Instrum. 58, 1601 (1987).
36. C. Keane, C. H. Nam, L. Meixler, H. Milchberg, C. H. Skinner, S. Suckewer, and D. Voorhees, Rev. Sci. Instrum. 57, 1296 (1986).